Bioorganic Chemistry 114 (2021) 105054

Contents lists available at ScienceDirect

Bioorganic Chemistry

journal homepage: www.elsevier.com/locate/bioorg

Revisiting ageless antiques; synthesis, biological evaluation, docking simulation and mechanistic insights of 1,4-Dihydropyridines as anticancer agents

Peter A. Sidhom [a,*], Eman El-Bastawissy [a], Abeer A. Salama [b], Tarek F. El-Moselhy [a]

[a] Department of Pharmaceutical Chemistry, Faculty of Pharmacy, Tanta University, Postal code: 31527, Tanta, Egypt
[b] Pharmacology Department, National Research Centre (NRC), 33 El Bohouth St. (Former El-Tahrir St.), Postal code:12622, Dokki, Giza, Egypt

ARTICLE INFO

Keywords:
1,4-Dihydropyridines
Anticancer
Mechanistic insight
Docking simulation
Synthesis
Enzyme inhibition assay

ABSTRACT

The historic DHP nucleus was serendipitously discovered by Arthur Hantzsch about 130 years ago and is still considered a hidden treasure for various pharmacological activities. Twenty-one DHP analogues were synthesized using the expedient one pot Hantzsch synthesis for screening as anticancer agents. Initially, the in vitro anti-proliferative single dose against a panel of 18 cancer cell lines showed that compounds **11b** and **8f** were the superlative candidates regarding their antitumor effect (GI% mean = 66.40% and 50.42%, correspondingly) compared to cisplatin (GI% mean = 65.58%) and doxorubicin (GI% mean = 74.56%). Remarkably, compound **11b** showed a remarkable MDA-MB-468 anticancer activity (GI%=80.81%), higher than cisplatin (64.44%) and doxorubicin (76.72%), as well as strong antitumor activity against lung cancer A549 (GI%= 83.02%), more powerful than both cisplatin and doxorubicin. Compound **11b** exhibited an exceptional anticancer activity against lung cancer cell line (A549) as its GI_{50} in nanomolar was (540 nM) with a 9-fold increase greater than cisplatin (GI_{50} = 4.93 μM) and with a selectivity index = 131 to cancer cells over normal cells. Further mechanistic investigations proved that DHPs anticipate simultaneously TOPI and RTKs (VEGFR-2, HER-2 and BTK) which can stimulate BAX/BAK and the executioner caspases via rtPCR studies.

1. Introduction

The eminent 1,4-dihydropyridine (DHP) nucleus was coined by Arthur Hantzsch in 1882 as an easily isolated intermediate in the parent Hantzsch pyridine synthesis [1-3]. Since then, this reaction has been fruitfully exploited in the synthesis of 1,4-DHPs and bears his name as "Hantzsch dihydropyridine synthesis". DHPs left the flask to become real life analgesic and spasmolytic agents in 1940 [4], then Bayer produced the crown jewel, nifedipine, in 1975 as a calcium channel blocker (CCB) for treatment of coronary artery disease [5]. Concurrently, the discovery of voltage-gated calcium channels (VGCCs) and their utility in coronary artery disease occurred by chance in 1953, when Paul Fatt and Bernard Katz left the Na^+ out of their bathing medium and found that the muscle still generated action potentials [6].

Extensive studies were conducted on calcium channels [7-10], until Fleckenstein (1983) depicted the discovery and use of verapamil, and the 1,4-DHPs including nifedipine, as antihypertensive drugs. Their target was found to be inhibition of cardiovascular calcium channels; thus, the term calcium channel blocker or antagonist was coined [11-14]. Thenceforth, about twenty clinically approved calcium channel blockers have been introduced to the market, most recently, Clevidipine, approved by the FDA in 2008.

DHP nucleus has proven to be a pharmacologically privileged scaffold, exhibiting diverse biological activities, such as anticancer [15-17], anticonvulsant [18-20], antidiabetic [21-23], anti-inflammatory agents [24,25], as well as in the management of Alzheimer disease [26].

Cancer is a large group of diseases that can start in almost any organ or tissue of the body when abnormal cells grow uncontrollably, go beyond their usual boundaries to invade adjoining parts of the body and/or spread to other organs. The latter process is called metastasizing

Abbreviations: **DHP**, **1,4-dihydropyridine**; **CCB**, **calcium channel blocker**; **VGCCS**, **voltage-gated calcium channels**; **MCRS**, **multicomponent reactions**; **TMD**, **2,2,6-trimethyl-1,3-dioxin-4-one**; **UDP**, **up-and-down**; **RTK**, **receptor tyrosine kinase**; **SI**, **selective index**; ***SEC***, **Solid Ehrlich Carcinoma**; **EAC**, **Ehrlich ascites carcinoma**; **CADD**, **Computer Aided Drug Design**; **PAINS**, **Pan-Assay Interference Compounds**.

* Corresponding author.
E-mail address: Peter.ayoub@pharm.tanta.edu.eg (P.A. Sidhom).

https://doi.org/10.1016/j.bioorg.2021.105054
Received 19 March 2021; Received in revised form 9 May 2021; Accepted 1 June 2021
Available online 4 June 2021

and is a major cause of death from cancer. Cancer is the second leading cause of death globally, accounting for an estimated 9.6 million deaths, or one in six deaths, in 2018. Lung, prostate, colorectal, stomach and liver cancer are the most common types of cancer in men, while breast, colorectal, lung, cervical and thyroid cancer are the most common among women [27].

The cancer burden continues to grow globally, exerting tremendous physical, emotional and financial strain on individuals, families, communities and healthcare systems. Many healthcare systems in low and middle-income countries are the least prepared to manage this burden. Approximately 70% of deaths from cancer occur in low and middle-income countries. Only 1 in 5 low and middle-income countries have the necessary data to drive cancer policy. In Egypt, about 128,892 cancer cases were counted in 2018 with 85,432 cancer deaths according to WHO-Cancer Country Profiles [28].

The accessible and prevailing anticancer drugs have distinctive mechanisms of action which ultimately make variations in their effects on heterogenous types of cancer and normal cells. In addition, there is insufficient evidence of biochemical alterations between normal cells and cancerous cells and hence, a particular cure for cancer has demonstrated indefinable. The evolution of resistance to existing multidrug chemotherapy and their less than desirable cure rate, dreadful and deleterious effects on patients are serious and pragmatic concerns. Hence, the impeccable effort required in an attempt to identify newer, efficient and less toxic chemotherapeutic agents for treating cancer [29].

Numerous reports have deliberated the anticancer effect of DHPs. Almost all of them correlated the anticancer power with the interruption of multidrug resistance (MDR), the primary cause of chemotherapy failure. DHPs exhibit remarkable inhibitory action on P-glycoprotein, one of the MDR mediators. This information also shows that the main trigger of the MDR inhibition of DHPs is due to being analogous to ATP in structure as well as the ability to be inserted in the ATP pocket [30-36].

None of these reports investigated the inherent cytotoxic activity of DHPs. Could DHPs act as intrinsic anticancer agents? Could calcium blocking activity have an impact? Could ATP structure similarity provoke a receptor tyrosine kinase (RTK) inhibition?

Some cancers are associated with the up-regulation of specific Ca^{2+} channels or pumps. Many Ca^{2+} channels, pumps and exchangers are modulated by pharmacological agents and are regarded as druggable. The role of Ca^{2+} in both proliferation and apoptosis means that both inhibitors, such as DHPs, and activators of these proteins are potential therapeutic agents in cancer chemotherapy. Simply, proliferation needs high intracellular concentration of Ca^{2+} and decreasing it ceases the tumorigenesis cascade [37]. The significance of increased expression of Ca^{2+} channels and pumps in cancer is directly related to the tumorigenic significance of the pathways regulated by Ca^{2+}. Moreover, unlike many of the ubiquitously expressed potential anticancer drug targets (such as regulators of the cell cycle), many of the Ca^{2+} channels and pumps with altered expression in cancer have a highly restricted tissue distribution [38,39]. Therefore, is the calcium channels blocking activity of DHPs a bane or a boon as anticancer agents?

To answer these questions, we synthesized 21 DHPs with different side chains and aldehydic-based cores, to evaluate their biological actions extensively via enzymatic assays, cell lines and *in vivo* studies. Moreover, biochemical parameters and histopathological examination were used. Furthermore, a proposed structure activity relationship was conducted to develop a paradigm for future drug discovery and open the gates for repositioning DHP nucleus in new druggable areas.

2. Results and Discussion

2.1. Chemistry

Twenty-one diverse compounds were synthesized in this research work. Symmetric and asymmetric DHPs were synthesized by Hantzsch condensation and Meyer modification, respectively. Another source of sundry was the use of 5 different aromatic aldehydes (piperonal, 2,3-methylenedioxy-benzaldehyde, fluorene-2-carboxaldehyde, 2,2-difluoro-1,3-benzodioxole-4-carbaldehyde and 1,4-benzodioxan-6-carboxaldehyde) and 6 different β-ketoesters (methyl, ethyl, isopropyl, tertbutyl, methoxy ethyl and benzyl acetoacetate) to create our series, besides two types of aminocrotonates (the methyl and ethyl derivatives) for Meyer *et al.* asymmetric DHP synthesis [40].

One approach to address the swift assembly of molecular diversity paradigm involves the development of multicomponent reactions (MCRs). In addition to the intrinsic atom economy and selectivity underlying such reactions, simpler procedures and equipment, time and energy savings, as well as environmental friendliness have all led to a sizable effort to design and implement MCRs in both academia and industry. The usefulness of MCRs is even greater if they provide access to "privileged medicinal scaffolds" [41]. Hantzsch synthesis of dihydropyridines could be an epitome of this paradigm.

Different acetoacetate derivatives (**2a-f**) were prepared according to the modified Clemens method [42] via condensation of 2,2,6-trimethyl-1,3-dioxin-4-one (TMD) with commercially available alcohols (**1a-f**) in refluxing xylene (Scheme 1) [43].

The prepared compounds (**2a-f**) were characterized by their melting points and compared with the reported values in Supporting Information Table S1.

Our offspring DHPs were divided into 4 series according to the type of aldehyde used in their synthesis. Series I shown in Scheme2 was composed of 7 compounds (**4a-e**) and (**6a,b**) based on piperonal, series II presented in Scheme 3 contained 8 compounds (**8a-f**) and (**9a,b**) based on 2,3-methylenedioxy-benzaldehyde, series III displayed in Scheme 4 comprised 3 compounds (**11a-c**) based on fluorene-2-carboxaldehydeandseries IV demonstrated in Scheme 5 included 3 compounds (**13a-c**) based on 1,4-benzodioxan-6-carboxaldehyde.

Different solvents could be used in the Hantzsch DHP synthesis, such as methanol, ethanol, isopropanol or water. Isopropanol was selected for our bench work as a solvent based on the high yield obtained. As a rationalization, the lipophilicity of the used aldehydes needs relatively moderately polar alcohols for dissolving and less polar ones for recrystallization to initiate seeding of crystals effortlessly.

2.2. Biological evaluation

2.2.1. Acute toxicity

The up-and-down (UDP) method was the one chosen in our work. The oral acute toxicity assay resulted in no lethality, manifestations of toxicity or any negative behavioral changes to motor activity, for all compounds up to a dose level of 2000 mg/kg over a period of 14 days. Hence, they were considered safe and the median lethal dose (LD_{50}) of our candidates was determined to be more than 2000 mg/kg body weight.

The UDP testing approach is the toxicological testing approach most recommended by various regulatory agencies because this method reduces the number of vertebrate animals in research. The UDP screening method involves dosing single animals sequentially at 48 h intervals. A dose less than the best-estimate LD_{50} dose is selected and administered to an animal, and the animal is observed for 48 h. If it survives, the study

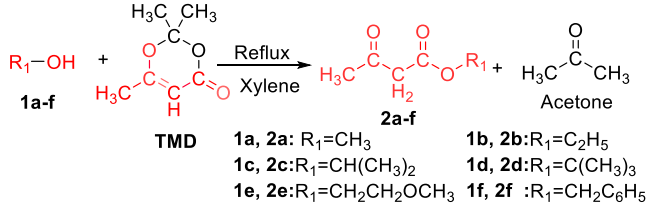

Scheme 1. Synthesis of **2a-f**.

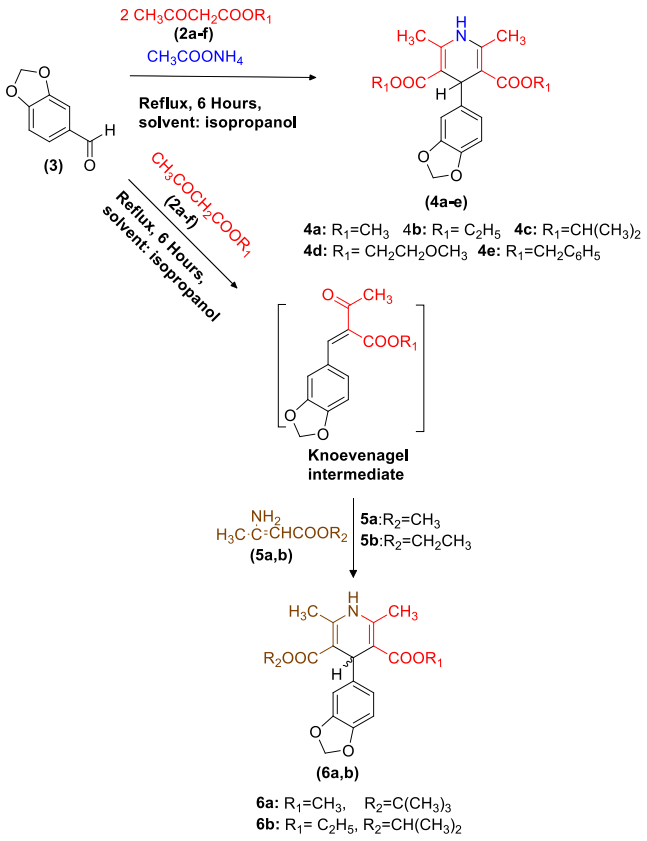

Scheme 2. Synthesis of **4a-e** and **6a,b**.

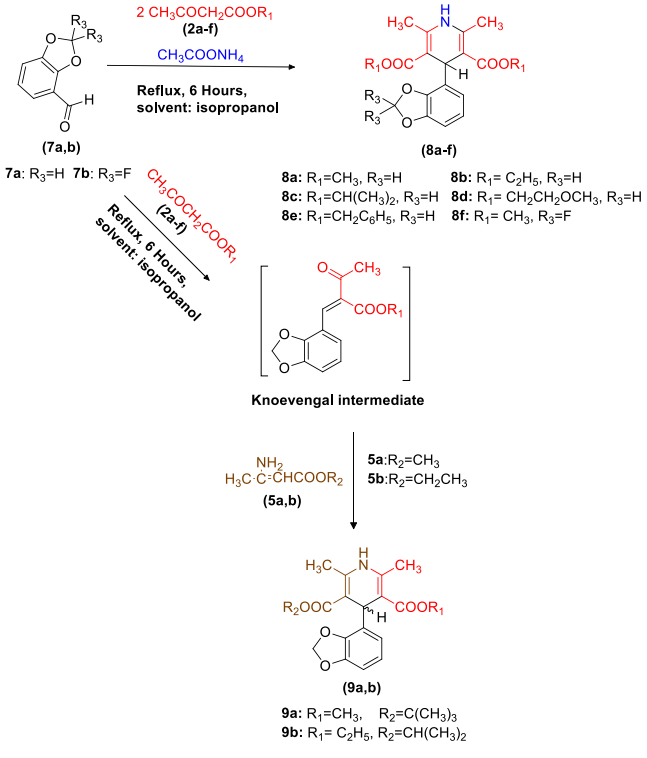

Scheme 3. Synthesis of **8a-e** and **9a,b**.

is continued with a higher dose (twice the original dose); if the animal dies, testing is conducted with a lower dose on another animal of the same sex as the original animal. UDP testing is limited to doses up to

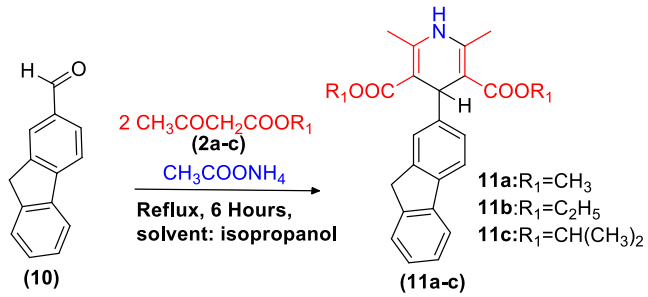

Scheme 4. Synthesis of **11a-c**.

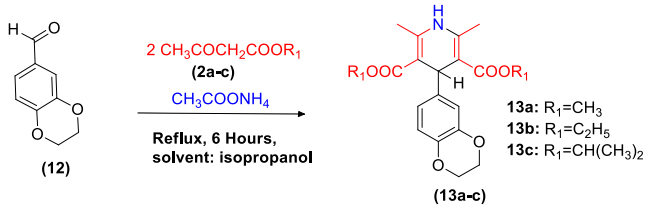

Scheme 5. Synthesis of **13a-c**.

2000 mg/kg [44].

2.2.2. Anticancer activity assessment

To give a comprehensive picture of DHPs anticancer mechanism, we designed our enterprise stepwise (Supporting Information Figure S1).

2.2.2.1. In vitro One-Dose Antiproliferative Screening and SAR Study. In an attempt to evaluate the effect of DHPs on cancer cell growth inhibition, we evaluated all synthesized compounds together with the reference compounds, cisplatin and doxorubicin, for their anti-proliferative activity in a panel of 18 human cancer cell lines of diverse malignancy types; leukemia (HL-60), lung cancer (A549), colorectal cancer (HT-92 and HCT-116), CNS cancer(SH-SY5Y), lymphoma (BC3), renal cancer (UO-31), prostate cancer (PC-3), pancreatic cancer (PANC-1), urinary bladder cancer (T-24), thyroid cancer(TT), cervical carcinoma (Hela), skin cancer (A431), liver cancer (Hep-G2), uterine cancer (DX-5 and MES-SA) and breast cancer (MCF-7 and MDA-MB-468), in order to detect their growth inhibition percentages (GI%) at a single dose concentration (10 μM) on cancer cell lines. Additionally, the mean-graph midpoint values ($GI\%_{mean}$) were described. The results are shown in (Supporting Files Table S7). To appraise the anticancer spectrum broadness, we assigned the number of susceptible cell lines for each compound. The cell line was selected as susceptible if the GI% was above 50% (Supporting Information Table S7).

Assessment of Table S7 bared a preliminary map for the strength and spectrum of the DHPs anticancer activity. Various compounds (**4b**, **8a, 8b**, **8f**, **9b**, **11b**, **11c**, **13a** and **13c**) exhibited strong anticancer activity (GI% higher than 70%), explained by the mean anticancer activity of compounds. Two compounds (**8f** and**11b**) showed broad spectrum activity (more than 11 susceptible cell lines), while other were less broad (**4b**, **8c**, **9b** and **11c**). Scrupulously, compounds **4a** and **4c** exhibited strong anticancer activity against MCF-7 cell line (GI%=74.99 and 70.29, respectively), although compounds **4b**, **6a**, **6b**, **8a**, **8c**, **8f**, **9a**, **9b, 11a**, **11b**, **13b** and **13c** only showed moderate activity (GI% ranged 51–67%). Compound **11b** showed a remarkable MDA-MB-468 anticancer activity (GI%=80.81%) even higher than cisplatin (64.44%) and doxorubicin (76.72%). Compounds **4a**, **4e**, **8a**, **8d**, **8f**, **11c** and **13b** showed moderate activity (GI% ranged 51–66.8%) on the same cell line, whilst compounds **4b**, **8b**, **8d** and **11b** showed strong antitumor activity against lung cancer A549 (GI%=70.16, 72.50, 70.09 and 83.02%, respectively). The outstanding compound **11b** inhibited A549 more

powerfully than both cisplatin and doxorubicin.

Conclusively, **11b** and **8f** were the superlative candidates regarding their antitumor effect (GI% mean = 66.40% and 50.42%, correspondingly), as well as concerning spectrum broadness (16 and 13 susceptible cell lines, respectively) (Fig. 1). In addition, the most susceptible cancer cell lines for DHPs were breast, lung, colorectal, skin, liver, leukemia and cervical carcinoma (Fig. 2).

To construct a more comprehensive SAR study, the safety of our candidate compounds should be considered. The in vitro one-dose antiproliferative assay was extended to involve nine human normal cell lines of various systems (Supporting Information Table S9). Surprisingly, all our candidates were safer on all human cells tested compared to cisplatin and doxorubicin. The most innocuous candidates were **4e**, **8c** and **11b**. Remarkably, there were two human cell lines that were tremendously vulnerable to cytotoxicity of DHPs (HEK-293 and FHC cell lines). Unfortunately, DHPs only exerted a weak effect on renal cancer cells and therefore, renal cancer was omitted from the anticancer spectrum of DHPs. Compound **11b** was more anodyne than **8f** on normal human cell lines (GI% mean = 22.80% and 34.99%, correspondingly).

Hence, **11b** was nominated for further investigation of selectivity examination and mechanistic insight.

SAR Prognostication

Regarding the aldehydic-based core, via comparing the potency of the four series, series III flaunted the utmost potency ($GI\%_{mean}$ = 52.6%), followed by series IV ($GI\%_{mean}$ = 45.30%), then series II ($GI\%_{mean}$ = 45.26%) and finally series I ($GI\%_{mean}$ = 44.01%). This reflects the role of the lipophilic core on enhanced potency. Changing the aldehydic core did not show a specific pattern in the anticancer spectrum broadness. Concerning safety to human cell lines, enhancing lipophilicity of the aldehydic core showed improved safety. This was presented by assessing GI% of **4b** and **11b** ($GI\%_{mean}$ = 32.14% and 22.80%, respectively) compared to **4a** and **11a** ($GI\%_{mean}$ = 38.38% and 34.54%, respectively). Comparing **8f** to the correspondent **8a**; adding an electron withdrawing group exhibited an improvement in activity ($GI\%_{mean}$ = 50.42% and 47.42%, respectively) and spectrum broadness (13 and 8 susceptible cell lines, correspondingly), but unfortunately these came with a decline in safety ($GI\%_{mean}$ = 34.99% and 32.76%, respectively).

Focusing on the side arms **4b**, **8f**, **9b**, **11b** and **11c** showed the highest antitumor activity (Fig. 1); reflecting that methyl, ethyl and isopropyl groups could be tolerated within the side arms. The *tert*-butyl group showed diminished activity to a large extent as in **6a** and **9a**, which were the least active compounds within the study ($GI\%_{mean}$ = 39.19% and 39.77%, respectively). The lipophilic benzyl side chain lessened the activity compared to aliphatic side chains, like in **4e** and **8e** ($GI\%_{mean}$ = 43.60% and 43.72%, respectively). Concerning the spectrum, the ethyl side arm showed a wider spectrum compared to the

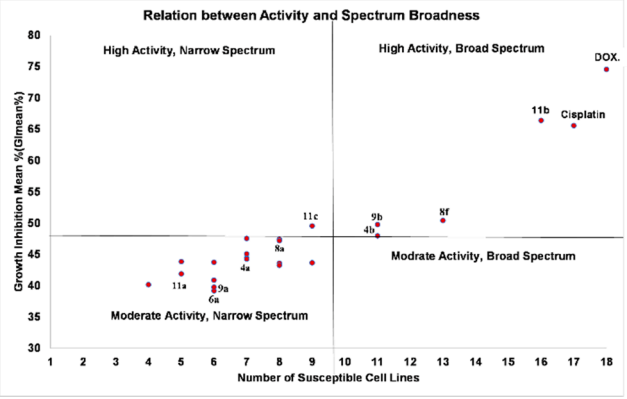

Fig. 1. Cross presentation to correlate the anticancer activity and spectrum broadness of candidate DHPs.

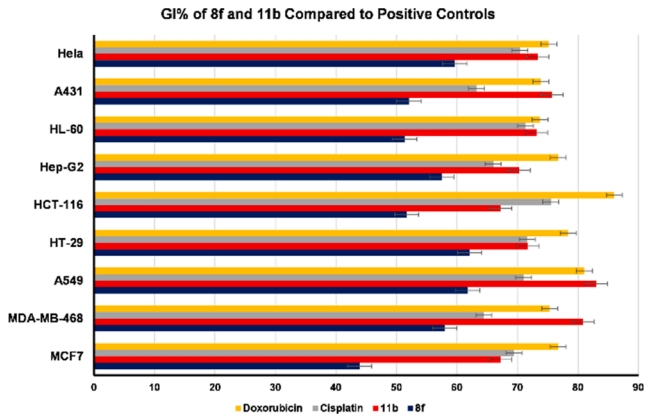

Fig. 2. GI% of **8f** and **11b** against most susceptible cancer cell lines.

methyl one, like in **4b** compared to **4a** (11 and 7 susceptible cell lines, correspondingly), **11b** compared to **11a** (16 and 5 susceptible cell lines, correspondingly) and **13b** compared to **13a** (8 and 7 susceptible cell lines, correspondingly). The *tert*-butyl group narrowed the spectrum as in **6a** and **9a** (6 susceptible cell lines for each). The lipophilic benzyl side chain tapers the spectrum compared to the aliphatic side chains, like in **4e** and **8e** (8 and 6 susceptible cell lines, correspondingly). Regarding safety to human cell lines, increasing the number of carbon atoms in the side arm generally showed improved safety. This presented by assessing GI% of **4a-e** ($GI\%_{mean}$ = 38.38, 32.14, 30.14, 29.75 and 24.63%, respectively). Despite that, the ethyl side arm is optimal (Supporting Information Figure S2).

These results indicate that compound **11b** can be considered as a potential lead compound for future development of broad-spectrum anticancer agents.

2.2.2.2. In Vitro Cytotoxicity Screening (GI_{50}) Against Cancer and Human Normal Cell Lines and Selectivity Index (SI). The benchmark for selectivity of a compound depends upon its selective index (SI) towards the other cancer cell lines, which was obtained by dividing the full panel GI_{50}mean (the average GI_{50} of all cell lines towards the test agent) by its individual GI_{50} (the GI_{50} of a specific cell line towards the test agent). The ratios between 3 and 6 indicate moderate selectivity, ratios greater than 6 refer to high selectivity to the corresponding cell line and compounds with ratios less than 3 will be non-selective towards the corresponding cell line [45]. Moreover, another eminent SI is the one that relates the cancer and normal cell lines. It is calculated as GI_{50} for normal cells/GI_{50} for cancer cells. It is accepted that the tested compound which has SI value more than three exhibits selective cytotoxicity towards the cancer cells rather than the normal cells, while the compound which has SI value less than three exhibits general toxicity for cancer and normal cells [46].

The results (Supporting Information Table S10 and Figure S3) showed some remarkable observations. Compound **11b**exhibited an exceptional anticancer activity against lung cancer cell line (A549) as its GI_{50} in nanomolar was (540 nM) with a 9-fold increase greater than cisplatin (GI_{50} = 4.93 μM). It also displayed powerful anticancer activity against breast cancer cell lines MCF-7 (GI_{50} = 1.08 μM) with a 4.5-fold increase over cisplatin and slightly higher than doxorubicin, (GI_{50} = 4.59 μM and GI_{50} = 1.36 μM, respectively) and MDA-MB-468 (GI_{50} = 1.08 μM) with a 6.5-fold increase over cisplatin and 2-fold increase more than doxorubicin, (GI_{50} = 6.99 μM andGI_{50} = 2.16 μM, respectively). Moreover, cervical carcinoma was targeted by **11b** (GI_{50} = 1.21 μM) with a 6-fold increase over cisplatin and 2.5-fold increase over doxorubicin, (GI_{50} = 7.26 μM and GI_{50} = 2.88 μM, respectively).

Moderate selectivity for thyroid and uterine cancer was also found (SI = 4.34 and 3.85, correspondingly) compared to cisplatin (SI = 1.0 and 1.50, correspondingly) and doxorubicin (SI = 3.46 and 2.37,

correspondingly) (Fig. 3). The greatest effect of compound **11b** was found to be against skin cancer cell line (GI_{50} = 1.38 μM) with a 6-fold increase over cisplatin and 1.5-fold increase more than doxorubicin, (GI_{50} = 8.09 μM and GI_{50} = 1.97 μM, respectively) and leukemia cell line (GI_{50} = 1.76 μM) with a 7-fold increase over cisplatin and 1.5-fold increase more than doxorubicin, (GI_{50} = 11.81 μM andGI_{50} = 2.88 μM, respectively).

Clearly compound **11b** had a profound effect on skin carcinoma and leukemia compared to other cancer types (SI = 20, 10.00, 9.00, 8.00 and 6.00, correspondingly), compared to cisplatin (SI = 2.00, 2.00, 1.50, 1.32 and 1.00, correspondingly) and doxorubicin (SI = 4.75, 2.5, 1.18, 1.73 and 1.19, correspondingly).

Regarding toxicity to human normal cells, the GI_{50} results of **11b** are posted in (Supporting Information Table S11). Compound **11b** showed extremely high selectivity to breast cancer (SI = 161) and lung cancer (SI = 114) rather than their human normal cell lines. Also, very high selectivity to cervical carcinoma (SI = 36) was found rather than its human normal cell line (Fig. 4)

Conclusively, **11b** proved its anticancer activity against lung and breast cancer with a higher safety profile to normal cells compared to cisplatin and doxorubicin. Therefore, the next question to be answered; how do DHPs perform this action?.

2.2.2.3. Mechanistic Insight of 11b-Induced Cytotoxicity in Breast and Lung Cancer. Our mechanistic hypothesis was built on deeper investigation of four cornerstones: cell cycle analysis and its regulators (CDKs), DNA topology (topoisomerases), cell proliferative oncogenes (RTKs) and other targets involved in tumorigenesis and apoptosis induction (pro-apoptotic and apoptotic markers).

Cell Cycle Analysis:

To explore the role of DHPs in the cell cycle of cancer cells, the most vulnerable cell lines were selected A549 (lung cancer) and MDA-MB-468 (breast cancer). These cells were treated with **11b**, cisplatin and doxorubicin at the same dose level (2 μM). The results are imparted in Table 1.

Compound **11b** induced apoptosis through aggregation of both A549 and MDA-MB-468 cells in G2/M transition. Interruption of pre-G1 phase was also observed (Supporting Information Figure S4 and S5).

Hence, **11b** should be submitted for CDK inhibition assay to confirm the G2/M cell arrest property. Two types of CDKs were chosen, CDK1 and CKD6 which regulate G2/M transition and G1 phase, respectively [47].

Surprisingly, **11b** inhibited both CDK1 and CDK6 at nM scale. **11b** showed more powerful inhibition to CDK1 than CDK6. This reflected that DHPs arrest the cell cycle of cancer cells at G2/M checkpoint rather than at the pre-G1 phase (Table 2).

DNA Topology

Assessing the topoisomerase inhibition activity of **11b** was needed to reveal the ability to induce DNA breaks and trigger the apoptosis pathways. There are two types of topoisomerases (TOP1 and TOP2).

***%Potency was calculated as ((IC_{50} reference/IC_{50} 11b) *100).**

TOP1 action is mainly related to G2/M checkpoint, while TOP2 works mainly in G1/S transition [48].

The results (Table 3) showed that **11b** had a comparable activity to camptothecin in TOP1 inhibition, but a much weaker activity to TOP2 compared to etoposide. These results confirmed the G2/M arrest, besides providing a cause to initiate apoptosis pathways via accumulation of DNA cleavable complexes due to inhibition of TOP1 activity.

Cell Proliferative Oncogenes (RTKs) and Other Targets Involved in Tumorigenesis.

The next piece of the assessment puzzle was the core of the mechanistic insight, composed of 7 RTKs (VEGFR2, HER1, HER2, HER3, BTK, JAK-3 and mTOR), enzyme assays and 3 other targets (Proteasome, Kinesin enzyme and PARP-1) involved in tumorigenesis. The results are showed in Table 4 and Table 5.

Table 4 showed that DHPs did not rely on proteasome, Kinsen and PARP1 targets in their anticancer activity, as **11b** exhibited very low enzyme inhibition compared to the reference drugs.

However, DHPs exhibited moderate to high enzyme inhibition power on selected RTKs as in Table 5. Compound **11b** showed moderate enzyme inhibition to HER-1 and HER-3. It also displayed strong enzyme inhibition to BTK and HER-2, as well as higher selectivity for HER-1 and HER-2 over other tested RTKs (Table 6).

Surprisingly, **11b** blocked the VEGFR-2 more sturdily than the reference (staurosporine, which is a pan RTK-inhibitor that can induce apoptosis in research work), as shown from their IC_{50}s. The obvious explanation for this multi-RTK inhibition could be the structure similarity of DHPs to ATP; the basis of DHPs early discovery [49], which could allow DHPs to block the ATP binding site of these RTKs. Inhibition of these RTKs hinders the tumorigenesis and induces cell apoptosis by

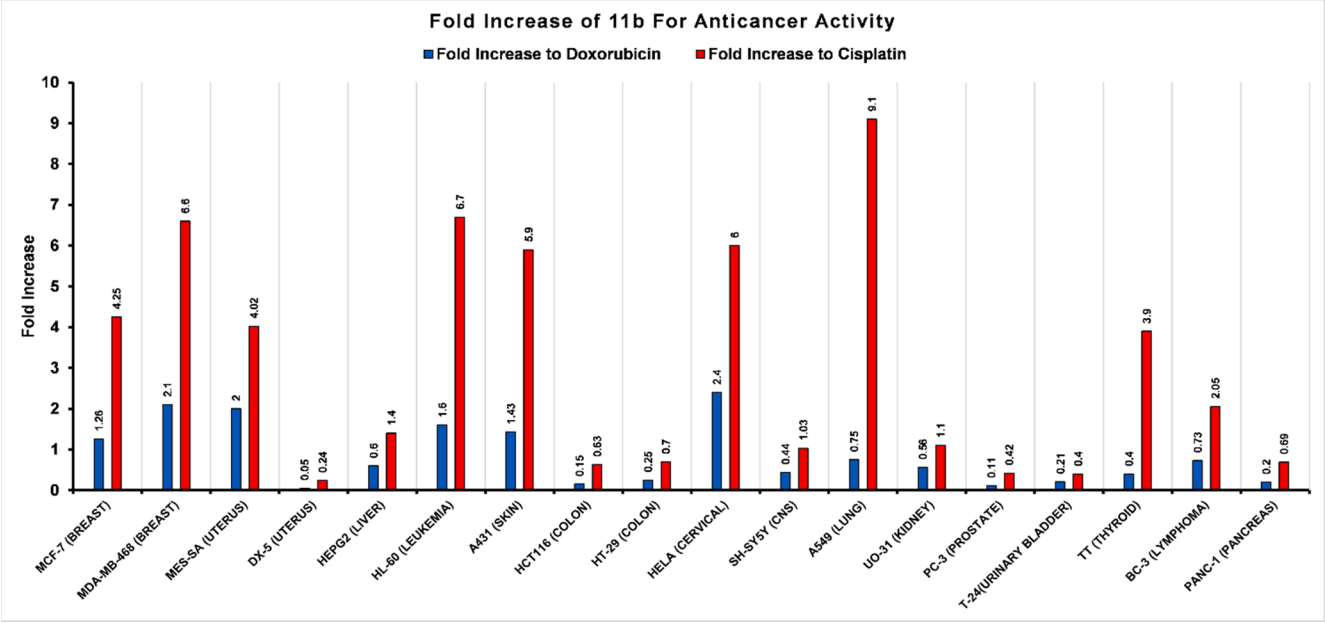

Fig. 3. Bar chart showing the comparison of compound **11b** against cisplatin and doxorubicin.

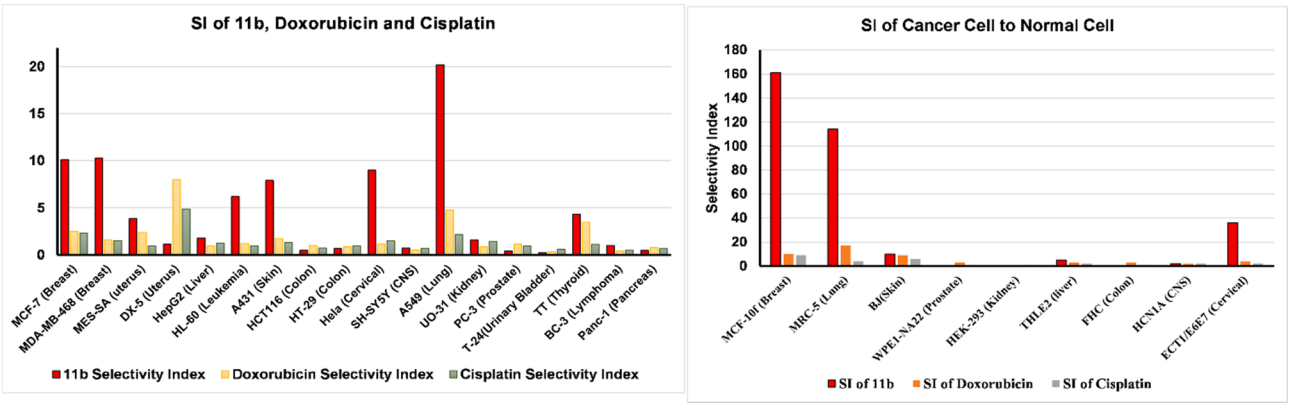

Fig. 4. (left) Selectivity index of **11b** for the anticancer activity over cisplatin and doxorubicin in an 18-cancer cell lines panel. (right) Selectivity index of **11b** for cancer cell over normal cell of the same type compared to cisplatin and doxorubicin.

Table 1
Effect of **11b**, cisplatin and doxorubicin on cell cycle phases in A459 and MDA-MB-468 cell lines.

Compound	Cell Cycle Distribution Percent				
		G0-G1 Transition	S Phase	G2/M Transition	Pre-G1 Phase
11b	A549	34.52	23.94	41.54	27.26
Cisplatin		39.78	25.36	34.86	18.43
Doxorubicin		26.77	31.52	41.71	32.49
Control		47.29	31.92	20.79	2.09
11b	MDA-MB-468	41.22	26.51	32.27	19.82
Cisplatin		37.52	28.51	33.97	16.37
Doxorubicin		29.76	24.38	45.86	25.74
Control		52.21	35.46	12.33	1.61

Table 2
IC_{50} of **11b** on CDK1 and CDK6 in nM ± SEM.

Compound	IC_{50} for CDK1	IC_{50} for CDK6
11b	19.12 ± 1.06	91.35 ± 1.41
Roniciclib	7.20 ± 0.389	38.26 ± 2.63

Table 3
IC_{50} of **11b** on TOP1 and TOP2 in μM/nM ± SEM.

Compound	IC_{50}/ TOP1	IC_{50}/TOP2
11b	670.95 ± 4.71 nM	292.45 ± 4.77 μM
Camptothecin	668.10 ± 5.59 nM	———
Etoposide	———	130.25 ± 4.08 μM

Table 4
IC_{50} of **11b** on proteasome, kinesin, PARP-1 and VEGFR-2 in nM ± SEM.

Compound	IC_{50} for Target Inhibition (nM)			
Name	Proteasome	PARP1	Kinesin	VEGFR-2
11b	298.99 ± 1.95	226.92 ± 3.88	557.02 ± 3.26	90.99 ± 2.55
% potency*	24.60	8.43	45.13	135.67
Bortezomib	73.54 ± 1.23	———	———	———
Olaparib	———	19.12 ± 0.41	———	———
Monastrol	———	———	251.38 ± 1.99	———
Staurosporine	———	———	———	122.84 ± 2.55

blocking several signaling pathways in the cancer cells, (Fig. 6).

Detection of Apoptosis

The mitochondrial pathway is closely regulated by a group of proteins belonging to the Bcl-2 family. One branch of this group, which includes mammalian Bcl-2, is anti-apoptotic by blocking the mitochondrial release of cyt C, over expression of which promotes tumorigenesis. In contrast, two other subgroups of the Bcl-2 family, termed Bax and Baf, can function as tumor suppressors by promoting the release of cyt C, required for apoptotic cell death [50].

Furthermore, p53 (the guardian of the genome) is a transcriptional factor that can initiate apoptosis in response to DNA damage and hyperproliferative signals [51]. p53 is disabled in most tumors, if not all, as a tumor-protective mechanism from apoptosis and provoking genome instability. The caspases or in other words the executioners of apoptosis are regulated by these proapoptotic factors.

The ultimate piece of the mechanistic puzzle was to examine the DHPs influence on cancer cell apoptosis. The previous puzzle pieces substantiated the induction of apoptosis either by accumulation of DNA cleavable complexes or multi-RTKs blocking effect. Hence, the expressions of apoptotic and anti-apoptotic markers were necessitated measurements (Table 7 and Table 8).

Compound **11b** elevated the level of proapoptotic Bax gene expression higher than cisplatin and was comparable to doxorubicin in both A549 and MDA-MB-468. Similarly, p53 gene expression was elevated in both A549 and MDA-MB-468 (Table 7).

To comprehend the DHPs-induced apoptosis, the executioner caspase-3 and caspase-9 concentrations should be appraised (Table 8). Compound **11b** elevated the levels of both caspase-3 and caspase-9 in A459 and MDA-MB-468 (8.5-fold and 5.37-fold, respectively) to higher levels than cisplatin (7.7-fold and 4.9-fold, respectively).

To quantify the apoptosis rate, we used Annexin V/PI method (Table 9). Compound **11b** induced early apoptosis in both A549 and MDA-MB-468 at 48 h (5.29% and 6.21%, respectively) compared to cisplatin (4.92% and 3.82%, respectively) and doxorubicin (7.29% and 6.12%, respectively). Compound **11b** also showed an enhanced late apoptotic induction in A549 and MDA-MB-468 (more than 62-fold and 41-fold over the untreated cells, respectively). Comparatively, cisplatin achieved more than 32-fold late apoptosis over the untreated cells in both cancer cell lines, whereas doxorubicin exhibited more than 70-fold and 64-fold over the untreated cells, respectively. Total induced apoptosis by compound **11b** in A594 and MDA-MB-468 was 24-fold and 23-fold higher than in the untreated cells, respectively. This total apoptosis induction was higher than treatment with cisplatin (14-fold and 16-fold higher than the untreated cells, respectively) and comparable to those treated with doxorubicin (24-fold and 30-fold higher than the untreated cells, respectively).

Table 5
IC_{50} of **11b** on RTKs in nM ± SEM.

Compound	IC_{50} for Enzyme Inhibition (nM) (RTKs) compared with Erlotinib					
Name	BTK	EGFR	HER-2	HER-3	JAK-3	mTOR
11b	68.80 ± 0.02	71.79 ± 2.96	84.51 ± 4.02	103.92 ± 4.50	987.38 ± 7.6	150.68 ± 2.21
Erlotinib	59.41 ± 0.02	49.13 ± 1.52	74.73 ± 3.99	66.44 ± 3.99	302.71 ± 2.5	71.83 ± 1.41
%potency*	86.10	68.44	88.40	62.00	30.60	47.67

*%potency was calculated as ((IC_{50} reference/IC_{50} 11b) *100)

Table 6
SI of **11b** on RTKs compared to erlotinib.

Compound	Selectivity Index*						
Name	BTK	EGFR (HER-1)	HER-2	HER-3	JAK-3	mTOR	IC_{50}mean
11b	0.92	3.96	3.36	2.74	0.29	1.89	284.35
Erlotinib	0.53	2.80	1.84	2.07	0.45	1.92	137.70

* SI was calculated as (IC_{50}mean/ IC_{50} 11b) for the same enzyme assayed.

2.2.2.4. Anti-Tumor Assay In Vivo. Based on the promising biochemical, cellular and pharmacodynamic properties, **11b** was subjected to anti-tumor evaluation *in vivo* using the Solid Ehrlich Carcinoma (*SEC*) xenograft model. The *SEC* model induced in mice was inaugurated as an indorsed model commonly used to investigate different chemotherapeutic treatment strategies for breast cancer. This model reflects a high degree of malignancy due to its high virulence, rapid development and highly infiltrative nature [52]. A previous study showed that Ehrlich ascites carcinoma (EAC) cells were a representative model for HER-2 positive breast cancer which suited our proposed pharmacodynamics of DHPs [53].

The *SEC* xenograft model in mice was established and the tumor-bearing mice were treated 2 days/week with intra-peritoneal (I.P.) injection of cisplatin and doxorubicin at a dose of 10 mg/kg, respectively, as positive controls. Animal groups received **11b** at a dose of 5, 10 and 15 mg/kg, respectively. All treatments were started from the12th day to the 28th day post-implantation. Tumor volume change during the experiment and tumor weights after euthanasia were recorded. Tumor growth inhibitions (TGIs) were also calculated post euthanasia.

Compound **11b** showed a substantial dose dependent decrease of the tumor volume at all recording intervals from the initial point to the 16th day-endpoint, compared to the vehicle control group. The 15 mg administered dose of **11b** exhibited strong tumor growth inhibition, higher than cisplatin and comparable to doxorubicin (Fig. 5c).

The TGI values revealed that the effect of **11b** increased gradually with dose elevation, notably the 15 mg dosage had a greater effect than

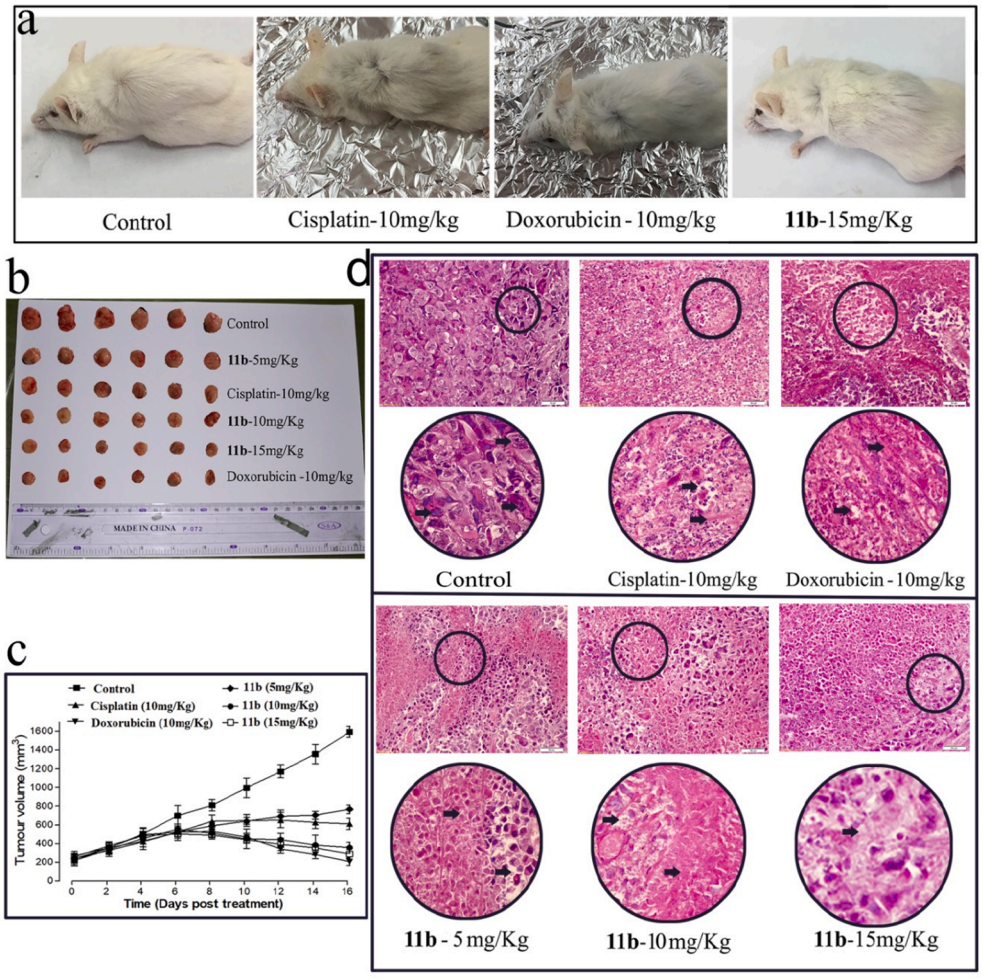

Fig. 5. Inhibited tumor growth of (*SEC*) xenograft model in mice. (a) External mice morphology showing the deleterious effects of cisplatin and doxorubicin compared to the higher safety profile of **11b.** (b) Tumors removed from the vehicle, cisplatin, doxorubicin, and **11b**-treated mice groups. (c) Tumor volume changes during 16 days of treatment. (d) Histopathological findings of the *SEC* sections stained with H&E (×200 and 400). The untreated mice showing cellular details of the tumor; the cells are polymorphic in shape, containing relatively large, highly chromatophilic nuclei with one or more prominent nucleoli; giant tumor cells are also seen (arrows). Cisplatin treated mice showing viable tumor cells surrounded by a layer of edema and inflammatory cells (arrows). Doxorubicin treated mice showing necrotic tumor cells with dystrophic calcifications surrounded by a layer of inflammatory cells (arrows). Compound **11b** treated mice showing a dose dependent antitumor behavior with strong necrotic patches with no viable tumor cells (arrows).profile compared to the deteriorated external profile of the mice treated with cisplatin and doxorubicin.

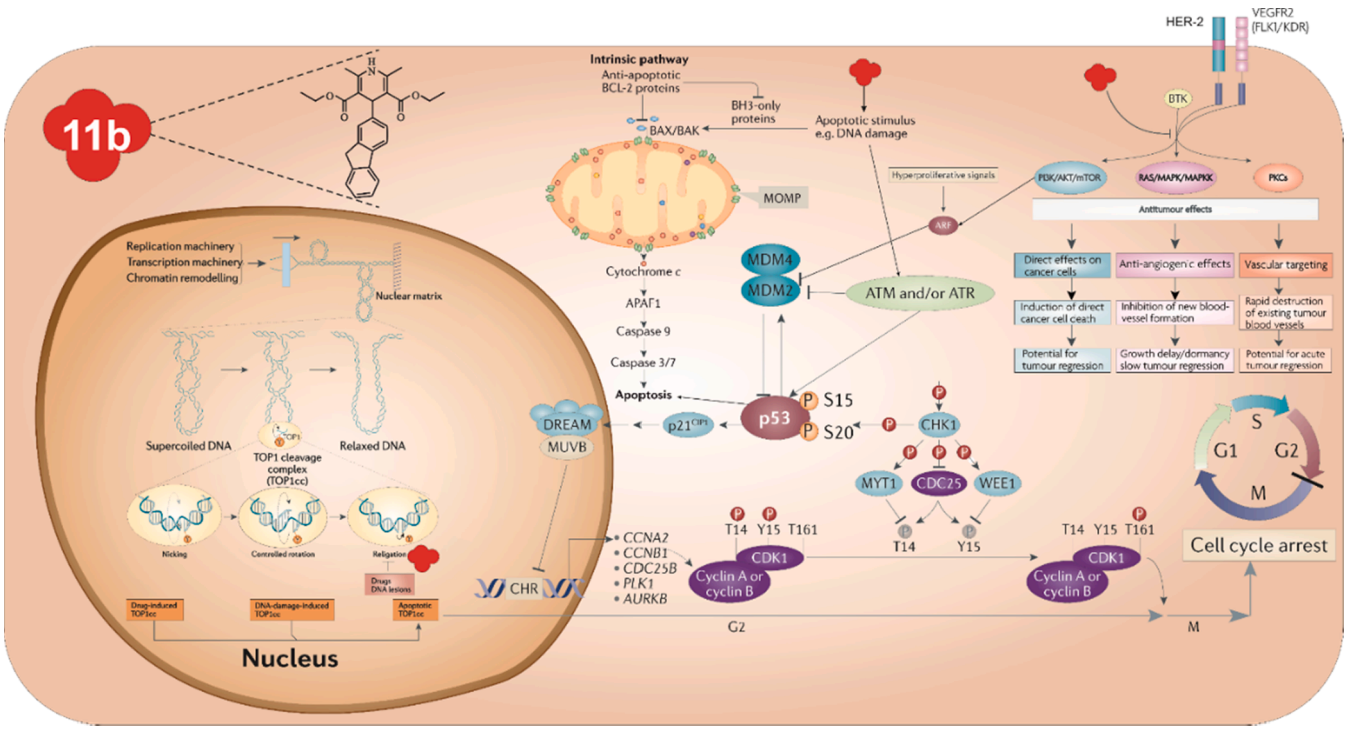

Fig. 6. Proposed molecular mechanism of 1,4-DHPs as anticancer agents.

Table 7
Measurement of fold increase in gene expression of proapoptotic factors by rtPCR for **11b**, cisplatin and doxorubicin-treated A549 and MDA-MB-468 cancer cell lines.

Compound		Proapoptotic Factors Gene Expression (Fold Increase)		
		Bax	Bcl-2	p53
11b	A549	5.49	0.22	6.53
Cisplatin		4.76	0.48	6.08
Dox		8.58	0.30	7.48
Control		1	1	1
11b	MDA-MB-468	6.49	0.54	9.49
Cisplatin		5.18	0.58	5.90
Dox		6.97	0.19	10.07
Control		1	1	1

10 mg cisplatin and was comparable to 10 mg-doxorubicin (Table 10). At the end of the treatment, all animals were euthanized and the *SEC* excised and weighed. Moreover, **11b** displayed a reduction in tumor weight compared to the vehicle control group in a dose dependent pattern. The percentage weight decrease of the 15 mg dosage of **11b** was higher than cisplatin and comparable to doxorubicin (74%, 48% and 81%, respectively) (Fig. 5b).

The visual external morphology of the treated mice with **11b** at a dosage of 15 mg showed a remarkable intact body (Fig. 5a).

Histopathological Examination

Histopathological examination of the *SEC* from the six groups revealed the typical picture of this type of tumor. Examination of sections prepared from the tumor tissue of the control group showed malignant cells with hyperchromatic nuclei, increased nucleo/cytoplasmic ratio, bizarre forms with pleomorphic changes and multi-nucleated

Table 9
Effect of **11b**, cisplatin and doxorubicin on apoptosis rate in A549 and MDA-MB-468 cell lines.

Compound		**Apoptosis**			**Necrosis**
		Total	**Early**	Late	
11b	**A549**	**24.91**	**5.29**	**19.63**	**2.34**
Cisplatin		**14.77**	**4.92**	**9.85**	**3.66**
Dox		**29.08**	**7.29**	**21.79**	**3.41**
Control		**1.02**	**0.71**	**0.31**	**1.07**
11b	**MDA-MB-468**	**16.91**	**6.21**	**10.7**	**2.91**
Cisplatin		**12.20**	**3.82**	**8.38**	**4.17**
Dox		**22.63**	**6.12**	**16.51**	**3.11**
Control		**0.75**	**0.49**	**0.26**	**0.86**

Table 8
Measurement of concentrations and fold increase in gene apoptotic caspases 3 and 9 for **11b**, cisplatin and doxorubicin-treated A549 and MDA-MB-468 cancer cell lines.

Compound		**Caspase-3**		**Caspase-9**	
		Concentration pg/ml ± SEM	**Fold Increase**	**Concentration ng/ml ± SEM**	**Fold Increase**
11b	**A549**	**362.2 ± 4.02**	**8.5**	**18.45 ± 0.19**	**11.3**
Cisplatin		**328.8 ± 9.82**	**7.7**	**17.13 ± 0.47**	**10.5**
Doxorubicin		**489.6 ± 18.3**	**11.5**	**26.56 ± 0.25**	**16.2**
Control		**42.52 ± 6.18**	**1.0**	**1.639 ± 0.16**	**1.0**
11b	**MDA-MB-468**	**389.8 ± 12**	**5.40**	**20.82 ± 0.25**	**7.4**
Cisplatin		**356.5 ± 11.72**	**4.90**	**18.94 ± 0.25**	**6.8**
Doxorubicin		**505.4 ± 9.72**	**7.0**	**29.13 ± 0.51**	**10.4**
Control		**72.56 ± 4.3**	**1.0**	**2.798 ± 0.44**	**1.0**

Table 10
Effect of **11b**, cisplatin and doxorubicin on tumor weight and TGI in *SEC* xenograft *in vivo* model.

Compound	Tumor Weight		TGI (%)
	Mean weight(g)±SEM	% Decrease	
11b (5 mg)	1.315 ± 0.14	41%	51.86
11b (10 mg)	0.89 ± 0.33	60%	77.65
11b (15 mg)	0.57 ± 0.21	74%	81.92
Cisplatin (10 mg)	1.15 ± 0.47	48%	61.71
Dox. (10 mg)	0.41 ± 0.29	81%	87.07
Vehicle Control	2.23 ± 0.95	———	——

tumor with giant cells, massive necrosis spread in solid sheets (H and E. × 400). Sections prepared from Group II (treated with10 mg of cisplatin) showed well-circumscribed tumor sections surrounded by edema and inflammatory cells. The presence of some viable tumor cells and a collar of inflammatory cellular filtrate and fibroblastic proliferation were observed. These findings support our previously recorded results of tumor volume measurements that showed cisplatin was efficient in restraining further tumor growth. In case of the mice treated with doxorubicin (10 mg), highly necrotic areas with no viable tumor cells were observed. Histopathological examination of Group IV-VI treated with **11b** revealed significantly different profiles in a concentration dependent manner.

Specimens showed no viable tumor cells, together with necrotic malignant cells with dystrophic calcification. Sections revealed mononuclear cellular infiltrate as well as macrophage infiltration of the necrotic tumor tissue. In addition, there was more massive patchy necrosis in the tumors with even eosin-stained proteins in the **11b** and doxorubicin-treated groups (Fig. 5d).

2.2.2.5. Calcium Channel Blocking Activity Assay. A major critique to the 1,4-DHP nucleus is the L/*T*-type calcium channel blocking activity which may cause some substantial side effects on the cardiovascular system. Hence, the nominated compound **11b** besides the second in the potency order **8f** were assessed for this issue to ensure its safety as anticancer agents.

Simply, our initiative was to select two cell lines with different levels of VGCCs expression. One possessed major expression of L-type and the other retained both L/*T*-type. Afterwards, we picked the neuroblastoma SH-SY5Y cells (containing L- and *T*-type Ca^{2+} channels) and the aortic smooth muscle A7r5 cells (containing L-type Ca^{2+} channels) of the rat. **11b** showed weak L and *T*-type calcium channels blocking activity while **8f,** the second in the order of the anticancer activity, exhibited a remarkably high L and *T*-type calcium channels blocking activity (Table 11). Conclusively, the anticancer action of 1,4-DHPs could depend on calcium channel blocking activity or not. Besides, weak calcium channel blocking activity of 1,4-DHPs (**11b**) could combine the anticancer effect with the higher safety margin by escaping from the eminent side effects of calcium channel blockers.

Table 11
The results of calcium overload-preventing activity (IC_{50}) of selected compounds in A7r5 and SHSY5Y cells(μM) ± SEM.

Compound	IC_{50}-A7r5 (μM)	*Fold Increase	Selectivity To L-Type VGCC**	IC_{50}-SH-SY5Y (μM)	*Fold Increase
8f	0.92 ± 0.02	3.31	14.51	13.53 ± 0.34	1.62
11b	6.37 ± 0.16	0.48	6.34	40.43 ± 1.02	0.54
Nifedipine	3.049 ± 0.07		7.19	21.92 ± 0.55	

*The fold increase over nifedipine is an indicator for biological activity enhancement, and it is calculated by (IC_{50} of nifedipine/IC_{50} of the compound in the same cell line).
**The selectivity index of L-type over *T*-type which is calculated by (IC_{50} of the compound in SH-SY5Y/ IC_{50} of the compound in A7r5).

2.3. Computer Aided Drug Design (CADD)

Our in-silico initiative was comprised of three keystones:

1) Prediction of pharmacokinetic properties of our lead compounds **11b** (the nominated anticancer DHP).
2) PAINS (Pan-Assay Interference Compounds) filtering.
3) Computational molecular docking to assess the binding modes of our lead compound to their mechanistic-predicted targets.

2.3.1. In-silico Pharmacokinetics and Prediction of Drug-likeness Properties

Generally, the SwissADME (absorption, distribution, metabolism and excretion) web tool [54] utilization showed that all our 21 candidates could passively be absorbed from the gastrointestinal tract (Supporting Information Figure S6 and Figure S7). Also, our candidates met all the drug-likeness criteria of Lipinski [55], Egan [56] and Muegge [57]. Moreover, our candidates had the physicochemical criteria for oral bioavailability and were located in the pink area of the radar diagram without any violations, except for **4e** and **8d**. Finally, all our candidates had a bioavailability score (0.55) and passed the PAINS filter (discussed later in Section 2.3.2.).

The physicochemical properties of the three lead compounds (Supporting Information Table S12) were located in the desired range of all the parameters. Penetration through the BBB (blood–brain barrier) depends on both the consensus log $P_{o/w}$ and the TPSA (topological polar surface area). Compound **11b** had consensus log $P_{o/w}$ value of 4.46 and TPSA value of 64.63. Interestingly, **11b** was found to have no violations in all drug-likeness rules (Veber [58], Lipinski, Ghose [59], Muegge, and Egan, and furthermore, when it comes to medicinal chemistry, none of the compounds exhibited any PAINS alerts.

2.3.2. PAINS Filters

In a move partially implemented to help editors and manuscript reviewers to rid the literature of PAINS (among other things), the Journal of Medicinal Chemistry encourages the inclusion of computer-readable molecular structures in the supporting information of submitted manuscripts, easing the use of automated filters to identify compounds' liabilities.

Being aware that nitro bearing 1,4-DHP dihydropyridines, such as nifedipine or nicardipine, have been recognized as putative PAINS or might also have the potential to form aggregates and cause misleading results. Hence, we conducted PAINS and aggregation filters to be confident about our designed candidates.

Initially, the analysis conducted by using SwissADME proved that none of our candidates were PAINS (as previously mentioned). Then, our lead compound **11b** were subjected to another two PAINS filters; the Free ADME-ToxFiltering Tool(Absorption, Distribution, Metabolism, Excretion and Toxicity) on the FAF-Drugs4 program (http://fafdrugs4.mti.univ-paris-diderot.fr/) and the "False Positive Remover" software (http://www.cbligand.org/PAINS/). Compound **11b** passed both filters as non-PAINS. Finally, **11b** was not recognized as aggregators according to the software "Aggregator Advisor" (http://advisor.bkslab.org/). These filter results confirmed that compound **11b** enzyme assays results were genuine with no false positive or negative results.

2.3.3. Computational Molecular Docking

The OEDocking v3.0.0 distribution using the FRED ligand shape fitting algorithm was utilized for receptor rigid body docking. All receptors used in this study were co-crystallized with ligands. The bound ligands were used to specify the active site. We saved the multiconformer ligand files in OEBinary, and therefore, there was no need to use the FRED conformer test flag. FRED was used with standard docking precision using 1.0 Å for the ligand translational step size and 1.5 Å for

the rotational step size.

Ligand sampling was a key factor in this case. OEDocking version 3.4.0.2 (FRED module) [60] under academic license used OMEGA version 3.1.2.2 [61] ligand conformational sampling as a predocking step, that allowed adding more flexibility during conformer generation. All 2D and 3D docking figures are displayed in the Supporting Information.

TOPI Docking

The structure of the human topoisomerase-IB (hTopIB) (PDB entry:1tl8) is composed of 765 amino acid residues and subdivided into four distinct domains: the *N*-terminal (1–214), the core (215–635), the linker (636–712), and the C-terminal domain (713–765). The *N*-terminal domain is 24 kDa and composed of 214 amino acids; it constitutes a highly protease-sensitive, hydrophilic, unstructured region of the hTopIB. The crystal structure is obtained with an *N*-terminal reduced active form of the enzyme in which the first 174 amino acids are missing. However, the X-ray density is only interpretable beginning from residue 215; therefore, the entire *N*-terminal domain is still not crystallized. The core domain consists of residues 215–635; it is involved in catalysis and important for the preferential binding of the enzyme to the super-coiled DNA. This domain contains all the catalytic residues (Arg^{488}, Lys^{532}, Arg^{590}, and His^{632}) except the active site Tyr^{723}. Based on the structure, this domain is further divided into three sub-domains. Sub-domains I (215–232 and 320–433) and II (233–319) form a "cap" region containing a pair of α-helices called the "nose cone". The core sub-domain III (434–635) forms the "cat" region. Opposite to the hinge (which is located at the top of sub-domain III) are two loops (called "lips") that interact with each other by six amino acids and one salt bridge (Lys^{369}-Glu^{497}), to close the enzyme around the DNA. HTopIB clamps around the DNA allowing the interaction of lips through a non-covalent interaction between the carboxylic lateral group of Glu^{497} and the side-chain amino group of Lys^{369}. Opening and closing of the protein clamp during DNA binding and release must involve the breaking of this interaction between the lips and the lifting of the cap away from the base. The topoisomerization reaction begins with the binding of hTopIB to the duplex DNA. For the binding to happen, the enzyme should initially exist in an "open" conformation, which is most likely achieved by a hinge-bending motion situated at the edge between core sub-domains I and III (residue Pro^{431}) and the boundary between helices 8 and 9 (residue Lys^{452}). The binding step occurs through the interaction of the charges present on the surface of the enzyme and DNA. This step culminates with the protein that completely embraces the DNA as a "clamp" such that the lips of core sub-domains I and III touch each other. As a result of this event, the active site residues are arranged in position for attacking the scissile phosphate, which leads to the cleavage of the strand and formation of the covalent attachment between the enzyme and the 3' end of the DNA [62].

Docking of compound **11b** and camptothecin initially revealed stronger binding of **11b** (-16.277 Kcal/mol) than camptothecin (-14.27 Kcal/mol). For camptothecin, it formed a hydrogen bond with Asn^{722} in the C-terminal region, as well as a critical hydrogen bond with catalytic Lys^{532} which proves that camptothecin works through blocking the active site of TOPI. On the other hand, compound **11b** worked via a completely different mode. It acted mainly in the core region except for the hydrophobic binding with Leu^{721}. Interestingly, compound **11b** formed a hydrophobic interaction with Pro^{431} keeping TOPI in the open state for a longer period and delaying the clamp state of the loops of the lips on the DNA duplex. Besides, compound **11b** stabilized its binding by hydrogen bond formation and strong hydrophobic interactions with the DNA duplex itself. Last but not least, the binding style of **11b** enabled a process of intercalation to the DNA base pairs hindering the function of TOPI. In simple words, compound **11b** did not form any interactions with the catalytic amino acids but it could still hinder the TOPI function by delaying the clamp state or intercalating the DNA duplex.

Protein Kinases (PK) Docking

Based on structural similarity between DHPs and ATP, we assumed that compound **11b** would act as an ATP-competitive inhibitor. Docking simulation was fulfilled to investigate this hypothesis and reveal the binding style in the ATP binding site of both serine-threonine kinases (such as, CDK1) and tyrosine kinases (such as, BTK, HER-2 and VEGFR-2).

CDK1 Docking

As mentioned before, compound**11b** could inhibit both CDK1 and CDK6 at nM scale but showed more powerful inhibition to CDK1 (29.12 ± 1.26 nM) than CDK6 (407.35 ± 9.41 nM), nearly 14-fold greater, which leads to the question of how compound **11b** interacted with CDK1.

The ATP binding site of CDK1 (PDB entry:4y72) is composed of 13 amino acid residues (Tyr^{15}, Lys^{33}, Val^{64}, Phe^{80}, Glu^{81}, Phe^{82}, Leu^{83}, Ser^{84}, Met^{85}, Asp^{86}, Asn^{133}, Leu^{135} and Asp^{146}) [63].

As expected, the binding style of compound **11b** was the anticipated salt-bridge between Lys^{33} and Glu^{51}formed in the CDK1 active site. Furthermore, the side chain of compound **11b** mimicked the adenine N1 of ATP and accepted a hydrogen bond from the backbone amide of Leu^{83}. The carbonyl group made a favorable hydrogen bond with the CDK1 backbone between Met^{85} and Asp^{86}. On the other side of the molecule, the ethyl side chain formed an edge-face pi-alkyl interaction with Tyr^{15} and occupied the active site behind the ribose binding site and overlapped the phosphate binding site.

BTK Docking

Several reported mutations of BTK have revealed the crucial role of certain amino acid residues in the ATP binding site. There are seven imperative amino acids in the ATP cleft (Leu^{408}, Gly^{414}, Tyr^{418}, Lys^{430}, Glu^{445}, Arg^{525} and Asn^{526}) [64,65].

Docking of compound **11b** into BTK (PDB entry: 4z3v) showed that the fluorene ring fitted in the hydrophobic pocket forming a network of interactions with $Leu^{408,}$ Val^{416}, Ala^{428} and Leu^{528}. Binding to Leu^{408} destabilized the beta conformation of the α-1 strand and disrupted its conformation placing residues 410–412 in a position which anticipated the triphosphate of ATP to bind to the BTK molecule. Meanwhile, compound **11b** interacted with Gly^{411} by hydrogen bonding through its carbonyl group, preventing ATP to enter its cleft. Based on the BTK structure, we propose that the transphosphorylation of Tyr551 can lead to BTK activation by triggering an exchange of hydrogen-bonded pairs from Glu^{445}/Arg^{544} to Glu^{44}/ Lys^{430} and subsequent relocation of the *N*-lobe. Surprisingly, compound **11b** formed a hydrogen bond with catalytic Lys^{430} via its esteratic oxygen and forestalled the triggering of BTK activation. On the contrary, erlotinib could not interact with the catalytic Lys^{430} which may have contributed to the comparable BTK inhibition activity of compound**11b** and erlotinib (IC_{50} = 307.80 nM and 261.41 nM, respectively). In other words, the powerful inhibition of BTK by compound**11b** stems from hindering ATP binding and transphosphorylation mediated activation.

HER-2 Docking

HER-2 is overexpressed in a number of human cancers, including 20–40% of solid tumors, e.g., breast, ovarian, lung, gastric, and oral cancers, in which over expression of this receptor correlates with poor prognosis.[9] In addition, because HER-2 is only expressed at low levels in normal human tissues, it is an attractive target for tumor-specific therapies. HER-2 adopts the typical kinase bilobed folding. The *N*-terminal lobe (*N*-lobe) contains mostly -strands and one α-helix, whereas the C-terminal lobe (C-lobe) is predominantly α-helical. The two lobes are connected by a flexible hinge region and separated by a deep cleft comprising the ATP binding site. The relative orientation of the two lobes has a distinct effect on the size of the ATP binding site, depending on the activation state of the kinase domain. Most of the residues associated with catalytic activity are located in the vicinity of the cleft, the glycine-rich nucleotide phosphate-binding loop (HER2: Leu726–Val734) and the α-helix C (αC; HER2: Pro761–Ala775) of the *N*-lobe of the kinase; and the DFG motif (HER2: Asp863–Gly865), the catalytic loop (HER2: Arg844–Asn850), and the activation loop (A-loop; HER2: Asp863–Val884) of the C-lobe of the kinase [66,67].

When compound **11b** interacted with HER-2 homodimer (PDB entry: 3RCD), a hydrogen bond interaction was clearly observed between the N—H group of the DHP core and the amine group of Arg^{849}. The length of this hydrogen bond was 3.0 A° indicating that the hydrogen bond was essential and strong for the inhibitory effect of **11b** on HER-2; particularly since Arg^{849} is part of the catalytic loop of HER-2. For the docking structures of a DHP analog **11b** with WT-HER-2, we confirmed that compound **11b** was well mapped in the ATP pocket of WT-HER-2. In the co-structure of compound **11b** with HER-2, the fluorene ring packed against α-helix C, making hydrophobic contact with the side chains of Val^{734}, Ala^{751}, Lys^{753} and Thr^{798}. These amino acids are near to the keychain of Asp^{863} in the DFG motif, which is important for inhibitor potency. In the hinge region, compound**11b** interacted with Met^{801} and the nearby Leu^{800} hydrophobically in the ATP binding site. Therefore, this suggestscompound**11b** might be an effective ATP-competitive HER-2 inhibitor.

VEGFR-2 Docking

The overall structure of VEGFR-2 in complex with sorafenib adopts a bilobar architecture characteristic of the eukaryotic protein kinase family. Situated in the cleft formed between the *N*-terminal and the C-terminal lobe, Lenvatinib binds to both the ATP-binding site (common sites for protein kinases) and the neighboring non-conserved allosteric region. X-ray analysis of the crystal structure of VEGFR2 − lenvatinib complex (PDB:3WZD) demonstrates that Lenvatinib is situated in the cleft between the two lobes. The amino acid residues located in the vicinity of Lenvatinib, at a maximum distance of 3.9 Å, belonged to the ATP-binding site (Leu^{840}, Gly^{841}, Ala^{866}, Glu^{885}, Val^{899}, Glu^{917}, Phe^{918}, Cys^{919}, Lys^{920}, Gly^{922}, Leu^{1035}, Cys^{1045} and Asp^{1046}), a gatekeeper residue (Val^{916}), and the neighboring region (Lys^{868}, Ile^{888}, Leu^{889}, Phe^{1047} and Leu^{1049}) [68].

By scrutinizing the binding mode of compound **11b** to VEGFR-2, a remarkable network of hydrophobic interactions was set up around the fluorene ring and ethyl side chains. Among the total 25 amino acid residues, 8 amino acid residues interacted with compound **11b** in its binding cleft. The fluorene ring had a conformation that allowed its interaction with gate keeper $Val^{916.}$ Moreover, the core fluorene ring of compound **11b** fitted into the ATP binding site via hitting Ala^{866}, Val^{899}, Leu^{1035} and Cys^{1045}. Also, compound **11b** bound to Cys^{919} of the ATP cleft by its ethyl side chain and Lys^{868} of the neighboring region. Therefore, compound **11b** completely occupied the adenine ring binding site and had strong hydrophobic interactions within the entrance region maintained by Val^{916}.The higher inhibition effect of compound **11b** over staurosporine (IC_{50} = 190.99 nM and 258.77 nM, respectively) can be explained by the higher docking score of **11b** (-12.51 Kcal/mol) compared to that of staurosporine (-9.63 Kcal/mol). The high docking score of compound **11b** arose from targeting the gate keeper Val^{916}.

3. Experimental Section

3.1. Chemistry

All organic reagents used were obtained from Sigma-Aldrich Company and were used without further purification. All candidates were synthesized in their racemic form (±) using the well-known Hantzsch three component reaction. Melting points were determined on an electro-thermal melting point apparatus (Stuart SMP10) by the open capillary method and were reported uncorrected. Reactions were monitored by thin layer chromatography (TLC) using pre-coated sheet (Fastman Kodak Co., Silica 60 F254) using developing systems: chloroform: isopropanol (90: 10) and were visualized with UV light at 254 nm. Elemental analysis (% C, H and N) was carried out by Perkin–Elmer 2400 CHNS analyzer and were within ± 0.40 of the theoretical values. IR spectra were recorded as KBr diluted pellets on a Jasco IR Spectrophotometer. Mass spectral data was obtained on GCMS (Schimadzu) QP-2010 plus using 70 eV for IE. ^{1}H, ^{13}C- NMR spectra were recorded on Bruker FT NMR spectrometer at 400 MHz (for ^{1}H NMR) and 100 MHz (for ^{13}C NMR) using $CDCl_3$ as a solvent. NMR spectra were reported in ppm downfield from tetramethylsilane. All chemical shift values, coupling constants, *J*, and multiplicity (s = singlet, d = doublet, dd = doublet of doublet, t = triplet, m = multiplet) were quoted in ppm and in Hz, respectively. Elemental analyses, ^{1}H, ^{13}C NMR and Mass spectra were performed by Micro Analytical Center, Faculty of Science, Cairo University, Giza, Egypt.

3.1.1. General Procedure for Preparation of Acetoacetates (2a-f)

A solution of the appropriate alcohol **1a-f** (25 mmol) and TMD (3.5 g, 25 mmol) in 10 ml xylene was heated under reflux in an oil bath at 150 °C, for 6 h. The reaction mixture was cooled and then xylene was removed under reduced pressure to yield products, **2a-f** of high purity, to be used immediately in subsequent reactions [192]. **2a**, yellow liquid, with bp 170–172 °C, (Reported bp 171 °C), **2b**, a yellow liquid, with bp 179–181 °C, (Reported bp 180 °C), **2c**, yellow liquid, with bp 186–188 °C, (Reported bp 185 °C), **2d**, yellow liquid, with bp 188–190 °C, (Reported bp 190 °C), **2e**, colorless liquid, with bp 189–191 °C, (Reported bp 192 °C), **2f**, colorless liquid, with bp 275–277 °C, (Reported bp 274 °C).

3.1.2. General Procedure for Preparation of DHP Derivatives (4a-e)

A mixture of acetoacetate esters **2a-f** (3.34 mmol), piperonal (0.250 g, 1.67 mmol) and ammonium acetate (0.162 g, 2.10 mmol) was dissolved in isopropanol (10 ml), and then heated under reflux for 6 h. The reaction mixture was quenched by the addition of dist. water (20 ml) and then cooled in an ice-bath. The precipitated solid was filtered and re-crystallized by methanol to afford products (**4a-e**).

*3,5-Dimethyl4-(2H-1,3-benzodioxol-5-yl)-2,6-dimethyl-1,4-dihydropyridine- 3,5-dicarboxylate (**4a**).*

Yield (0.495 g, 85.9%) as yellow crystals. R_f = 0.71 (chloroform: isopropanol (90: 10)); mp 197–198 °C. ^{1}HNMR (400 MHz, $CDCl_3$) δ (ppm): 2.34 (s, 6H, C_2-**CH_3**and C_6-**CH_3**), 3.68 (s, 6H, COO**CH_3**), 4.95 (s, 1H, C_4-**H**), 5.85 (s, 1H, N**H**), 5.90 (s, 2H, O**CH_2**O), 6.66 (d, *J* = 8.0 Hz, 1H, $C_{7'}$-**H**), 6.74–6.78 (m, 2H, $C_{4'}$-**H** and $C_{6'}$-**H**). ^{13}CNMR (100 MHz, $CDCl_3$) δ (ppm): 19.52 (2C, C_2-**CH_3**and C_6-**CH_3**), 39.02 (1C, **C_4**), 51.02 (2C, COO**CH_3**), 100.67 (1C, O**CH_2**O), 103.99 (2C, **C_3** and **C_5**), 107.77 (1C, **$C_{4'}$**), 108.26 (1C,**$C_{7'}$**), 120.59 (1C, **$C_{6'}$**), 141.72 (1C,**$C_{5'}$**), 144.05 (1C, **$C_{7a'}$**), 145.82 (2C, ***C_2*** and **C_6**), 147.30 (1C, aromatic **$C_{3a'}$**), 168.07 (2C, **2C = O**).IR (KBr disc):$\bar{\nu}$(cm^{-1}): 3342 (N—H Str), 2952 (aliphatic C—H Str), 1697 (C═O Str), 1649 (aliphatic C═C Str), 1489 (aromatic C═C), 1225 (aliphatic C—N Str), 749 (N—H Wag). EI-MS: *m/z* (% abundance): 344.85 (**M^+**, 8.57), 223.95 (**$M^+-C_7H_5O_2$**,100.00). Elemental analysis (%) for $C_{18}H_{19}NO_6$, calcd. (found):C 62.60 (62.50), H 5.55 (5.70), N 4.06 (3.78).

*3,5-Diethyl4-(2H-1,3-benzodioxol-5-yl)-2,6-dimethyl-1,4- dihydropyridine- 3,5-dicarboxylate (**4b**).*

Yield (0.570 g, 91%) as yellow crystals. R_f = 0.73 (chloroform: isopropanol (90: 10)); mp 141–143 °C.^{1}HNMR (400 MHz, $CDCl_3$) δ (ppm): 1.25 (t, *J* = 7.2 Hz, 6H, 2 of CH_2**CH_3**), 2.33 (s, 6H, C_2-**CH_3** and C_6-**CH_3**), 4.09 (q, *J* = 7.2 Hz, 4H, 2 of **CH_2**CH_3), 4.94 (s, 1H, C_4-**H**), 5.81 (s, 1H, **NH**) , 5.89 (s, 2H, O**CH_2**O), 6.65–6.86 (m, *J* = 4.8 Hz, 3H, $C_{7'}$-**H**,$C_{6'}$-**H** and $C_{4'}$-**H**). ^{13}CNMR (100 MHz, $CDCl_3$) δ (ppm): 14.28 (2C,CH_2**CH_3**), 19.51 (s, 2C, C_2-**CH_3**and C_6-**CH_3**), 39.32 (1C, **C_4**), 59.73 (2C, **CH_2**CH_3), 100.61 (1C, O**CH_2**O), 104.22 (2C, **C_3** and **C_5**), 107.54 (1C, **$C_{4'}$**), 108.57 (1C, **$C_{7'}$**), 120.96 (1C, $C_{6'}$), 142.06 (1C, **$C_{5'}$**), 143.71 (1C, **$C_{7a'}$**), 145.71 (2C, ***C_2*** and **C_6**), 147.18 (1C,**$C_{3a'}$**), 167.65 (2C, **2C = O**).IR (KBr disc): $\bar{\nu}$(cm^{-1}): 3298 (N—H Str), 2982 (aliphatic C—H Str), 1690 (C═O Str), 1645 (aliphatic C═C Str), 1495 (aromatic C═C), 1209 (aliphatic C—N Str), 794 (N—H Wag). EI-MS: *m/z* (% abundance): 372.85 (**M^+**, 12.79), 251.85 (**$M^+-C_7H_5O_2$**,100.00). Elemental analysis (%) for $C_{20}H_{23}NO_6$, calcd. (found), C 64.33 (64.50), H 6.21 (6.32), N 3.75 (3.40).

*3,5-Diisopropyl 4-(2H-1,3-benzodioxol-5-yl)-2,6-dimethyl-1,4-dihydropyridine-3,5-dicarboxylate (**4c**).*

Yield (0.477 g ,71.3%) as yellow crystals. R_f = 0.75 (chloroform: isopropanol (90: 10)); mp 196–197 °C.^{1}HNMR (400 MHz, $CDCl_3$) δ

(ppm): 1.08 (d, $J = 6.2$ Hz, 6H, CH($\mathbf{CH_3}$)$_2$), 1.17 (d, $J = 6.2$ Hz, 6H, CH($\mathbf{CH_3}$)$_2$), 2.24 (s, 6H, C_2-$\mathbf{CH_3}$ and C_6-$\mathbf{CH_3}$), 4.82 (s, 1H, C_4-**H**), 4.91 (m, $J = 6.5$ Hz, 2H, 2 of **CH**(CH$_3$)$_2$), 5.51 (s, 1H, NH) , 5.80 (s, 2H, O$\mathbf{CH_2}$O), 6.57 (d, $J = 8.0$ Hz, 1H, $C_{6'}$-**H**), 6.68 (s, 1H, $C_{4'}$-**H**) 6.70 (d, $J = 8.0$ Hz, 1H, $C_{7'}$-**H**). ^{13}CNMR (100 MHz, CDCl$_3$) δ (ppm): 19.59 (2C, C_2-$\mathbf{CH_3}$and C_6-$\mathbf{CH_3}$), 21.88 (2C, CH($\mathbf{CH_3}$)$_2$), 22.13 (2C, CH($\mathbf{CH_3}$)$_2$), 39.51 (1C, $\mathbf{C_4}$), 66.99 (2C, 2 of **CH**(CH$_3$)$_2$), 100.58 (1C, O$\mathbf{CH_2}$O), 104.63 (2C, $\mathbf{C_3}$ and $\mathbf{C_5}$), 107.37 (1C, $\mathbf{C_{4'}}$), 108.75 (1C,$\mathbf{C_{7'}}$), 121.21 (1C, $\mathbf{C_{6'}}$), 142.16 (1C, $\mathbf{C_{5'}}$), 143.21 (1C, $\mathbf{C_{7a'}}$), 145.64 (2C, $\boldsymbol{C_2}$ and $\mathbf{C_6}$), 147.09 (1C, $\mathbf{C_{3a'}}$), 167.14 (2C,2**C** = **O**). IR (KBr disc): $\tilde{\nu}$ (cm^{-1}): 3338 (N—H Str), 2981 (aliphatic C—H Str), 1696 (C═O Str), 1651 (aliphatic C═C Str), 1496 (aromatic C═C), 1216 (aliphatic C—N Str), 746 (N—H Wag). EI-MS: *m/z* (% abundance): 400.90 (**M**$^+$, 15.00), 279.90(**M**$^+$−$\mathbf{C_7H_5O_2}$,84.92), 237.90 (**M**$^+$−$\mathbf{C_{10}H_{11}O_2}$,40.56), 195.90 (**M**$^+$−$\mathbf{C_{13}H_{17}O_2}$,100.00). Elemental analysis (%) for$C_{22}H_{27}NO_6$, calcd. (found): C 65.82 (65.89), H 6.78 (6.69), N 3.49 (3.19).

*3,5-Bis(2-methoxyethyl) 4-(2H-1,3-benzodioxol-5-yl)-2,6-dimethyl-1,4-dihydropyridine-3,5-dicarboxylate (**4d**)*

Yield (0.608 g, 84%) as pale-yellow crystals. $R_f = 0.45$ (chloroform: isopropanol(90:10)); mp 114–116 °C.^{1}HNMR (400 MHz, CDCl$_3$) δ (ppm): 2.24 (s, 6H, C_2-$\mathbf{CH_3}$ and C_6-$\mathbf{CH_3}$), 3.31 (s, 6H, 2 of O$\mathbf{CH_3}$), 3.55 (t, $J = 5.0$ Hz, 4H, 2 of $\mathbf{CH_2}$OCH$_3$), 4.16 (t, $J = 5.0$ Hz, 4H, 2 of COO$\mathbf{CH_2}$), 5.11 (s,1H, C_4-**H**), 5.88 (s, 2H, O$\mathbf{CH_2}$O), 6.46 (s, 1H, NH), 6.60 (d, $J = 7.8$ Hz, 1H, $C_{6'}$-**H**), 6.65 (s, 1H, $C_{4'}$-**H**) 6.78 (d, $J = 7.7$ Hz, 1H, $C_{7'}$-**H**).^{13}CNMR (100 MHz, CDCl$_3$) δ (ppm): 19.56 (2C, C_2-$\mathbf{CH_3}$and C_6-$\mathbf{CH_3}$), 39.30 (1C, $\mathbf{C_4}$), 58.83 (2C, 2 of O$\mathbf{CH_3}$) , 62.81 (2C, 2 of COO$\mathbf{CH_2}$),70.63(2C, 2 of $\mathbf{OCH_2}$), 100.63 (1C, O$\mathbf{CH_2}$O), 104.09 (2C, $\mathbf{C_3}$ and $\mathbf{C_5}$), 107.61 (1C, $\mathbf{C_{4'}}$), 108.77 (1C, $\mathbf{C_{7'}}$), 121.00 (1C, $\mathbf{C_{6'}}$), 141.95 (1C, $\mathbf{C_{5'}}$), 144.08 (1C, $\mathbf{C_{7a'}}$), 145.76 (2C, $\boldsymbol{C_2}$ and $\mathbf{C_6}$), 147.17 (1C, $\mathbf{C_{3a'}}$), 167.47 (2C, 2**C** = **O**). IR (KBr disc): $\tilde{\nu}$(cm^{-1}): 3339 (N—H Str), 2946 (aliphatic C—H Str), 1690 (C═O Str), 1619 (aliphatic C═C Str), 1487 (aromatic C═C), 1208 (aliphatic C—N Str), 741 (N—H Wag). EI-MS: *m/z* (% abundance): 432.90 (**M**$^+$,7.64), 311.90 (**M**$^+$−$\mathbf{C_7H_5O_2}$,100), 253.90 (**M**$^+$−$\mathbf{C_{10}H_{11}O_3}$,18.87), 195.90 (**M**$^+$−$\mathbf{C_{13}H_{17}O_3}$,29.03). Elemental analysis (%) for $C_{22}H_{27}NO_8$, calcd. (found): C 60.96 (60.91), H 6.28 (6.53), N 3.23 (3.50).

*3,5-Dibenzyl 4-(2H-1,3-benzodioxol-5-yl)-2,6-dimethyl-1,4- dihydropyridine-3,5-dicarboxylate (**4e**)*

Yield (0.730 g, 88%) as pale-yellow crystals. $R_f = 0.91$ (chloroform: isopropanol(90:10));mp 67–69 °C.^{1}HNMR (400 MHz, CDCl$_3$) δ (ppm): 2.32 (s, 6H, C_2-$\mathbf{CH_3}$ and C_6-$\mathbf{CH_3}$), 5.04 (s, 1H, C_4-**H**), 5.12 (d, $J = 12.5$ Hz, 2H, COO$\mathbf{CH_2}$), 5.16 (d, $J = 12.5$ Hz, 2H, COO$\mathbf{CH_2}$), 5.90 (s, 2H, O$\mathbf{CH_2}$O), 6.14(s, 1H, NH), 6.63 (d, $J = 7.8$ Hz, 1H, $C_{6'}$-**H**), 6.70 (d, $J = 8.1$ Hz, 1H, $C_{7'}$-**H**), 6.76 (s, 1H, $C_{4'}$-**H**) , 7.27–7.33 (m, 10*H*, , 2 of $\mathbf{C_6H_5}$). ^{13}CNMR (100 MHz, CDCl$_3$) δ (ppm): 19.52 (2C, C_2-$\mathbf{CH_3}$and C_6-$\mathbf{CH_3}$), 39.48 (1C, $\mathbf{C_4}$), 65.71 (2C, 2 of COO$\mathbf{CH_2}$), 100.67 (1C, O$\mathbf{CH_2}$O), 103.92 (2C, $\mathbf{C_3}$ and $\mathbf{C_5}$), 107.64 (1C, $\mathbf{C_{4'}}$), 108.69 (1C, $\mathbf{C_{7'}}$), 121.16 (1C, $\mathbf{C_{6'}}$), 127.85 (4C , 2 of C_6H_5-$\boldsymbol{C_2}$ and $\mathbf{C_6}$), 127.93 (2C, 2 of C_6H_5-$\mathbf{C_4}$), 128.42 (4C, 2 of C_6H_5-$\mathbf{C_3}$ and $\mathbf{C_5}$), 136.51 (2C , 2 of C_6H_5-$\mathbf{C_1}$), 141.86 (1C, $\mathbf{C_{5'}}$), 144.49 (1C, $\mathbf{C_{7a'}}$), 145.85 (2C, $\boldsymbol{C_2}$ and $\mathbf{C_6}$), 147.30 (1C, $\mathbf{C_{3a'}}$), 167.44 (2C, 2**C** = **O**). IR (KBr disc): $\tilde{\nu}$ (cm^{-1}): 3345 (N—H Str), 2977 (aliphatic C—H Str), 1692 (C═O Str), 1650 (aliphatic C═C Str), 1488 (aromatic C═C), 1206 (aliphatic C—N Str), 751 (N—H Wag). EI-MS: *m/z* (% abundance): 496.85 (**M**$^+$,5.76), 405.85 (**M**$^+$−$\mathbf{C_7H_7}$,18.10), 375.85 (**M**$^+$−$\mathbf{C_7H_5O_2}$,98.12) 91.00 ($\mathbf{C_7H_7}$, 100.00). Elemental analysis (%) for $C_{30}H_{27}NO_6$, calcd. (found): C 72.42 (72.67), H 5.47 (5.82), N 2.82 (2.54).

3.1.3. General Procedure for Preparation of DHP Derivatives (*6a,b*)

A mixture of acetoacetate esters **2c, d** (1.67 mmol), piperonal (0.250 g, 1.67 mmol) and alkyl 3-aminocrotonate (1.67 mol) was dissolved in isopropanol (10 ml), and then heated under reflux for 6 h. The reaction mixture was quenched by the addition of dist. water (20 ml) and then cooled in an ice-bath. The precipitated solid was filtered and re-crystallized by methanol to afford products (**6a,b**).

3-*Tert*-butyl 5-methyl 4-(2H-1,3-benzodioxol-5-yl)-2,6-dimethyl-1,4-dihydropyridine-3,5-dicarboxylate (6a).

The general procedure mentioned above was applied using piperonal (0.250 g, 1.67 mmol), **2d** (0.264 g, 1.67 mmol) and methyl 3-aminocrotonate (0.192 g, 1.67 mmol) to afford 0.530 g, (82.1% yield) as pale-yellow crystals. $R_f = 0.84$ (chloroform: isopropanol (90:10)); mp 165–167 °C.^{1}HNMR (400 MHz, CDCl$_3$) δ (ppm): 2.26 (s, 9H, C ($\mathbf{CH_3}$)$_3$), 3.59 (s, 9H, C_2-$\mathbf{CH_3}$, C_6-$\mathbf{CH_3}$ and O$\mathbf{CH_3}$), 4.85 (s, 1H, $\mathbf{C_4}$-H), 5.57 (s, 1H, NH), 5.81 (s, 2H, O$\mathbf{CH_2}$O), 6.58 (dd, $J = 8.0$, 1.4 Hz, 1H, $C_{6'}$-**H**), 6.65–6.69 (m, 2H, $C_{4'}$-**H** and$C_{7'}$-**H**). ^{13}C NMR (CDCl$_3$) δ (ppm): 19.61 (2C, C_2-$\mathbf{CH_3}$and C_6-$\mathbf{CH_3}$), 28.33 (3C, C($\mathbf{CH_3}$)$_3$), 39.02 (1C, $\mathbf{C_4}$), 51.01 (1C, O$\mathbf{CH_3}$) , 88.81 (1C, **C**(CH$_3$)$_3$),100.67 (1C, O$\mathbf{CH_2}$O), 104.10 (2C, $\mathbf{C_3}$ and $\mathbf{C_5}$), 107.77 (1C, $\mathbf{C_{4'}}$), 108.28 (1C, $\mathbf{C_{7'}}$), 120.61 (1C, $\mathbf{C_{6'}}$), 141.69 (1C, $\mathbf{C_{5'}}$), 143.90 (1C, $\mathbf{C_{7a'}}$), 145.83 (2C, $\boldsymbol{C_2}$ and $\mathbf{C_6}$), 147.30 (1C, $\mathbf{C_{3a'}}$), 168.00 (2C, 2**C** = **O**). IR (KBr disc): $\tilde{\nu}$ (cm^{-1}): 3344 (N—H Str), 2977 (aliphatic C—H Str), 1692 (C═O Str), 1605 (aliphatic C═C Str), 1488 (aromatic C═C), 1247 (aliphatic C—N Str), 752 (N—H Wag). EI-MS: *m/z* (% abundance): **386.85** (**M**$^+$, 0.39), 223.85 ($\mathbf{C_{11}H_{13}NO_4^+}$,100). Elemental analysis (%) for $C_{21}H_{25}NO_6$, calcd. (found): C 65.10 (65.50), H 6.50 (6.60), N 3.62 (3.49).

*3-Ethyl 5-isopropyl 4-(2H-1,3-benzodioxol-5-yl)-2,6-dimethyl-1,4-dihydropyridine-3,5-dicarboxylate (**6b**).*

The general procedure mentioned above was applied using piperonal (0.250 g, 1.67 mmol), **2c** (0.241 g, 1.67 mmol) and ethyl 3-aminocrotonate (0.215 g, 1.67 mmol) to give 0.459 g, (71.01 %yield) as pale-yellow crystals. $R_f = 0.81$ (chloroform: isopropanol(90:10)); mp 170–172 °C.^{1}HNMR (400 MHz, CDCl$_3$) δ (ppm): 1.17 (d, $J = 6.3$ Hz, 6H, CH($\mathbf{CH_3}$)$_2$), 1.26 (t, $J = 7.4$ Hz, 3H, $CH_2\mathbf{CH_3}$), 2.34 (s, 6H, C_2-$\mathbf{CH_3}$ and C_6-$\mathbf{CH_3}$), 4.13 (q, $J = 7.1$ Hz,2H, $\mathbf{CH_2}$CH$_3$), 4.92 (s, 1H, C_4-**H**), 4.96–5.02 (m, $J = 6.5$ Hz, 1H, **CH**(CH$_3$)$_2$), 5.62 (s, 1H, NH) , 5.90 (s, 2H, O$\mathbf{CH_2}$O), 6.66 (d, $J = 8.0$, 1.4 Hz, 1H, $C_{6'}$-**H**), 6.76–6.80 (m, 2H, $C_{4'}$-**H** and$C_{7'}$-**H**). ^{13}CNMR (100 MHz, CDCl$_3$) δ (ppm): 14.29 (1C, $CH_2\mathbf{CH_3}$), 19.57 (2C, C_2-$\mathbf{CH_3}$and C_6-$\mathbf{CH_3}$), 22.12 (2C, CH($\mathbf{CH_3}$)$_2$), 39.43 (1C, $\mathbf{C_4}$), 59.71 (1C, $\mathbf{CH_2}$CH$_3$), 66.99 (1C, **CH**(CH$_3$)$_2$), 100.60 (1C, O$\mathbf{CH_2}$O), 104.71 (2C, $\mathbf{C_3}$ and $\mathbf{C_5}$), 107.45 (1C, $\mathbf{C_{4'}}$), 108.68 (1C, $\mathbf{C_{7'}}$), 121.10 (1C, $\mathbf{C_{6'}}$), 142.16 (1C, $\mathbf{C_{5'}}$), 143.22 (1C, $\mathbf{C_{7a'}}$), 145.68 (2C, $\boldsymbol{C_2}$ and $\mathbf{C_6}$), 147.14 (1C, $\mathbf{C_{3a'}}$), 167.13 (2C, 2**C** = **O**).IR (KBr disc):$\tilde{\nu}$ (cm^{-1}): 3337 (N—H Str), 2981 (aliphatic C—H Str), 1696 (C═O Str), 1652 (aliphatic C═C Str), 1494 (aromatic C═C), 1213 (aliphatic C—N Str), 745 (N—H Wag). EI-MS: *m/z* (% abundance): 386.90 (**M**$^+$,10.57), 343.85 (**M**$^+$−$\mathbf{C_3H_7}$, 18.38), 315.85 (**M**$^+$−$\mathbf{C_5H_{12}}$, 19.05), 265.95 (**M**$^+$−$\mathbf{C_7H_5O_2}$, 63.13), 195.90 (**M**$^+$−$\mathbf{C_{12}H_{17}O_2}$, 100). Elemental analysis (%) for $C_{21}H_{25}NO_6$, calcd. (found): C 65.10 (64.95), H 6.50 (6.50), N 3.62 (3.81).

3.1.4. General Procedure for Preparation of DHP Derivatives (*8a-f*).

A mixture of acetoacetate esters **2a-f** (3.34 mmol), 2,3-Methylenedioxy benzaldehyde (0.250 g, 1.67 mmol) and ammonium acetate (0.162 g, 2.10 mmol) was dissolved in isopropanol (10 ml), and then heated under reflux for 6 h. The reaction mixture was quenched by the addition of dist. water (20 ml) and then cooled in an ice-bath. The precipitated solid was filtered and re-crystallized by methanol to afford products (**8a-e**). The same procedure was applied in the synthesis of **8f,** but via using methyl acetoacetate (0.365 g, 3.16 mmol), 2,2-Difluoro-1,3-benzodioxole-4-carbaldehyde (0.250 g, 1.58 mmol) and ammonium acetate (0.162 g, 2.10 mmol).

*3,5-Dimethyl 4-(2H-1,3-benzodioxol-4-yl) −2,6-dimethyl-1,4- dihydropyridine-3,5-dicarboxylate (**8a**).*

Yield (0.547 g, 95%) as pale-yellow crystals. $R_f = 0.69$ (chloroform: isopropanol (90:10)); mp 208–210 °C. ^{1}H NMR (400 MHz, CDCl$_3$) δ (ppm): 2.32 (s, 6H, C_2-$\mathbf{CH_3}$and C_6-$\mathbf{CH_3}$), 3.65 (s, 6H, COO$\mathbf{CH_3}$), 5.13 (s, 1H, C_4-**H**), 5.86 (s, 1H, NH), 5.92 (s, 2H, O$\mathbf{CH_2}$O), 6.65 (d, $J = 8.0$ Hz, 1H, $C_{7'}$-**H**), 6.71 (t, $J = 8.0$ Hz 1H, $C_{6'}$-**H**), 6.77 (d, $J = 8.0$ Hz, 1H, $C_{5'}$-**H**). ^{13}C NMR (CDCl$_3$) δ (ppm): 19.36 (2C, C_2-$\mathbf{CH_3}$and C_6-$\mathbf{CH_3}$), 34.88 (1C, $\mathbf{C_4}$), 50.92 (2C, COO$\mathbf{CH_3}$), 100.41 (1C, O$\mathbf{CH_2}$O), 102.19 (2C, $\mathbf{C_3}$ and $\mathbf{C_5}$), 106.43 (1C, $\mathbf{C_{7'}}$), 121.09 (1C, $\mathbf{C_{5'}}$), 122.38 (1C, $\mathbf{C_{6'}}$), 129.48 (1C, $\mathbf{C_{4'}}$), 144.45 (2C, $\boldsymbol{C_2}$ and $\mathbf{C_6}$), 144.60 (1C, aromatic $\mathbf{C_{3a'}}$), 147.00 (1C, $\mathbf{C_{7a'}}$), 168.05 (2C, 2**C** = **O**). IR (KBr disc):$\tilde{\nu}$ (cm^{-1}): 3362 (N—H Str), 2943

(aliphatic C—H Str), 1706 (C═O Str), 1652 (aliphatic C═C Str), 1482 (aromatic C═C), 1218 (aliphatic C—N Str), 734 (N—H Wag). EI-MS: *m/z* (% abundance): 344.85 (**M^+**, 10.89), 223.95 (**$M^+-C_7H_5O_2$**,100.00). Elemental analysis (%) for $C_{18}H_{19}NO_6$, calcd. (found):C 62.60 (62.86), H 5.55 (5.35), N 4.06 (3.88).

*3,5-Diethyl4-(2H-1,3-benzodioxol-4-yl)-2,6-dimethyl-1,4-dihydropyridine-3,5-dicarboxylate (**8b**).*

Yield (0.520 g, 83%) as yellow crystals. R_f = 0.72 (chloroform: isopropanol (90: 10)); mp 151–153 °C.^{1}HNMR (400 MHz, $CDCl_3$) δ (ppm): 1.25 (t, *J* = 7.2 Hz, 6H, 2 of CH_2**CH_3**), 2.33 (s, 6H, C_2-**CH_3**and C_6-**CH_3**), 4.09 (q, *J* = 7.2 Hz ,4H, 2 of **CH_2**CH_3), 4.94 (s, 1H, C_4-**H**), 5.81 (s, 1H, **NH**) , 5.89 (s, 2H, O**CH_2**O), 6.62 (d, *J* = 7.9 Hz, 1H, $C_{7'}$-**H**), 6.70 (t, *J* = 7.9 Hz, 1H, $C_{6'}$-**H**), 6.76 (d, *J* = 7.9 Hz, 1H, $C_{5'}$-**H**).^{13}CNMR (100 MHz, $CDCl_3$) δ (ppm): 14.28 (2C,CH_2**CH_3**), 19.49 (2C, C_2-**CH_3**and C_6-**CH_3**), 39.32 (1C, **C_4**), 59.72 (2C, **CH_2**CH_3), 100.60 (1C, O**CH_2**O), 104.08 (2C, **C_3** and **C_5**), 107.53 (1C, **$C_{7'}$**), 120.94 (1C, **$C_{5'}$**), 122.50 (1C, **$C_{6'}$**), 128.29 (1C, **$C_{4'}$**), 142.13 (2C, ***C_2*** and **C_6**), 143.93 (1C, **$C_{3a'}$**), 147.10 (1C, **$C_{7a'}$**), 167.73 (2C, **2C = O**). IR (KBr disc): $\tilde{\nu}$(cm^{-1}): 3296 (N—H Str), 2983 (aliphatic C—H Str), 1688 (C═O Str), 1646 (aliphatic C═C Str), 1497 (aromatic C═C), 1207 (aliphatic C—N Str), 768 (N—H Wag). EI-MS: *m/z* (% abundance): 372.85 (**M^+**, 16.76), 251.90 (**$M^+-C_7H_5O_2$**,100.00). Elemental analysis (%) for $C_{20}H_{23}NO_6$, calcd. (found): C 64.33 (64.13), H 6.21 (6.12), N 3.75 (4.02).

*3,5-Diisopropyl 4-(2H-1,3-benzodioxol-4-yl)-2,6-dimethyl-1,4-dihydropyridine-3,5-dicarboxylate (**8c**).*

Yield (0.571 g, 85.3%) as yellow crystals. R_f = 0.74 (chloroform: isopropanol (90: 10)); mp 203–204 °C.^{1}HNMR (400 MHz, $CDCl_3$) δ (ppm): 1.08 (d, *J* = 6.2 Hz, 6H, CH(**CH_3**)$_2$), 1.17 (d, *J* = 6.3 Hz, 6H, CH (**CH_3**)$_2$), 2.24 (s, 6H, C_2-**CH_3** and C_6-**CH_3**), 4.82 (s, 1H, C_4-H), 4.91 (m, *J* = 6.4 Hz ,2H, 2 of **CH**(CH_3)$_2$), 5.13 (s, 1H, NH) , 5.80 (s, 2H, O**CH_2**O), 6.57 (d, *J* = 7.9 Hz, 1H, $C_{7'}$-**H**), 6.68 (t, *J* = 7.9 Hz, 1H, $C_{6'}$-**H**), 6.70 (d, *J* = 7.9 Hz, 1H, $C_{5'}$-**H**). ^{13}CNMR (100 MHz, $CDCl_3$) δ (ppm): 19.59 (2C, C_2-**CH_3**and C_6-**CH_3**), 21.88 (2C, CH(**CH_3**)$_2$), 22.13 (2C, CH(**CH_3**)$_2$), 39.51 (1C, **C_4**), 67.00 (2C, 2 of **CH**(CH_3)$_2$), 100.58 (1C, O**CH_2**O), 104.63 (2C, **C_3** and **C_5**), 107.37 (1C, **$C_{7'}$**), 121.52 (1C, **$C_{5'}$**), 122.65 (1C, **$C_{6'}$**), 129.54 (1C, **$C_{4'}$**), 144.53 (2C, ***C_2*** and **C_6**), 144.81 (1C, aromatic **$C_{3a'}$**), 147.12 (1C, **$C_{7a'}$**), 167.15 (2C, **2C = O**). IR (KBr disc): $\tilde{\nu}$(cm^{-1}): 3338 (N—H Str), 2981 (aliphatic C—H Str), 1696 (C═O Str), 1652 (aliphatic C═C Str), 1497 (aromatic C═C), 1217 (aliphatic C—N Str), 745 (N—H Wag). EI-MS: *m/z* (% abundance): 400.85 (**M^+**, 14.54), 279.90 (**$M^+-C_7H_5O_2$**, 86.72), 237.90 (**$M^+-C_{10}H_{11}O_2$**, 42.15), 195.90 (**$M^+-C_{13}H_{17}O_2$**, 100.00). Elemental analysis (%) for $C_{22}H_{27}NO_6$, calcd. (found): C 65.82 (66.05), H 6.78 (6.67), N 3.49 (3.66).

*3,5-Bis(2-methoxyethyl)4-(2H-1,3-benzodioxol-4-yl)-2,6-dimethyl-1,4-dihydropyridine-3,5-dicarboxylate (**8d**).*

Yield (0.655 g, 90.5%) as pale-yellow crystals. R_f = 0.40 (chloroform: isopropanol(90:10)); mp 123–125 °C.^{1}H NMR (400 MHz, $CDCl_3$) δ (ppm): 2.24 (s, 6H, C_2-**CH_3** and C_6-**CH_3**), 3.31 (s, 6H, 2 of O**CH_3**), 3.55 (t, *J* = 5.0 Hz, 4H, 2 of **CH_2**OCH_3), 4.16 (t, *J* = 5.0 Hz, 4H, 2 of COO**CH_2**), 5.11 (s,1H, C_4-**H**), 5.88 (s, 2H, O**CH_2**O), 6.46 (s, 1H, NH), 6.59 (d, *J* = 7.9 Hz, 1H, $C_{7'}$-**H**), 6.65 (t, *J* = 7.9 Hz, 1H, $C_{6'}$-**H**), 6.77 (d, *J* = 7.9 Hz, 1H, $C_{5'}$-**H**). ^{13}CNMR (100 MHz, $CDCl_3$) δ (ppm): 19.14 (2C, C_2-**CH_3**and C_6-**CH_3**), 39.25 (1C, **C_4**), 58.73 (2C, 2 of O**CH_3**) , 62.61 (2C, 2 of COO**CH_2**), 70.54 (2C, 2 of **OCH_2**), 100.34 (1C, O**CH_2**O), 104.12 (2C, **C_3** and **C_5**), 107.55 (1C, **$C_{7'}$**), 121.64 (1C, **$C_{5'}$**), 122.62 (1C, **$C_{6'}$**), 129.84 (1C, **$C_{4'}$**), 143.98 (2C, ***C_2*** and **C_6**), 145.70 (1C, **$C_{3a'}$**), 147.12 (1C, **$C_{7a'}$**), 167.35 (2C, **2C = O**). IR (KBr disc): $\tilde{\nu}$(cm^{-1}): 3336 (N—H Str), 2943 (aliphatic C—H Str), 1692 (C═O Str), 1651 (aliphatic C═C Str), 1489 (aromatic C═C), 1206 (aliphatic C—N Str), 751 (N—H Wag). EI-MS: *m/z* (% abundance): 432.80 (**M^+**,8.03), 311.90 (**$M^+-C_7H_5O_2$**,100), 253.90 (**$M^+-C_{10}H_{11}O_3$**,17.60), 195.90 (**$M^+-C_{13}H_{17}O_3$**,29.31). Elemental analysis (%) for $C_{22}H_{27}NO_8$, calcd. (found): C 60.96 (61.15), H 6.28 (6.34), N 3.23 (3.44).

*3,5-Dibenzyl4-(2H-1,3-benzodioxol-4-yl)-2,6-dimethyl-1,4-dihydropyridine-3,5-dicarboxylate (**8e**).*

Yield (0.647 g, 78%) as pale-yellow crystals. R_f = 0.89 (chloroform: isopropanol(90:10)); mp 78–79 °C.^{1}HNMR (400 MHz, $CDCl_3$) δ (ppm): 2.32 (s, 6H, C_2-**CH_3** and C_6-**CH_3**), 5.04 (s, 1H, C_4-**H**), 5.10 (d, *J* = 12.6 Hz, 2H, COO**CH_2**), 5.17 (d, *J* = 12.6 Hz, 2H, COO**CH_2**), 5.89 (s, 2H, O**CH_2**O), 6.14 (s, 1H, NH), 6.62 (d, *J* = 8.0 Hz, 1H, $C_{7'}$-**H**), 6.70 (t, *J* = 8.1 Hz, 1H, $C_{6'}$-**H**), 6.76 (d, *J* = 7.9 Hz, 1H, $C_{5'}$-**H**), 7.2–7.40 (m, 10*H*, 2 of **C_6H_5**). ^{13}CNMR (100 MHz, $CDCl_3$) δ (ppm): 19.52 (2C, C_2-**CH_3** and C_6-**CH_3**), 39.28 (1C, **C_4**), 65.71 (2C, 2 of COO**CH_2**), 100.67 (1C, O**CH_2**O), 103.91 (2C, **C_3** and **C_5**), 107.65 (1C, **$C_{7'}$**), 121.71 (1C, **$C_{5'}$**), 122.56 (1C, **$C_{6'}$**), 127.84 (2C, 2 of **C_6H_5**-C_4), 127.90 (4C , 2 of C_6H_5-**C_2** and **C_6**), 128.40 (4C , 2 of C_6H_5-**C_3**and **C_5**),130.12 (1C, **$C_{4'}$**), 142.00 (1C, **$C_{4'}$**), 144.31 (2C, ***C_2*** and **C_6**), 145.75 (1C, aromatic **$C_{3a'}$**), 147.25 (1C, **$C_{7a'}$**), 167.40 (2C, **2C = O**). IR (KBr disc): $\tilde{\nu}$(cm^{-1}): 3336 (N—H Str), 2944 (aliphatic C—H Str), 1692 (C═O Str), 1650 (aliphatic C═C Str), 1488 (aromatic C═C), 1206 (aliphatic C—N Str), 751 (N—H Wag). EI-MS: *m/z* (% abundance): 496.75 (**M^+**,4.26), 405.85 (**$M^+-C_7H_7$**,13.95), 375.90 (**$M^+-C_7H_5O_2$**,70.13), 91.00 (**C_7H_7**, 100.00). Elemental analysis (%) for $C_{30}H_{27}NO_6$, calcd. (found): C 72.42 (72.57), H 5.47 (5.64), N 2.82 (2.61).

*3,5-Dimethyl4-(2,2-difluoro-2H-1,3-benzodioxol-4-yl)-2,6-dimethyl-1,4-dihydropyridine-3,5-dicarboxylate (**8f**).*

Yield (0.498 g, 82.7%) as pale-yellow crystals. R_f = 0.67 (chloroform: isopropanol (90:10)); mp 214–216 °C. ^{1}HNMR (400 MHz, $CDCl_3$) δ (ppm): 2.37 (s, 6H, C_2-**CH_3**and C_6-**CH_3**), 3.64 (s, 6H, COO**CH_3**), 5.20 (s, 1H, C_4-**H**), 5.68 (s, 1H, NH), 6.86 (d, *J* = 7.7 Hz, 1H, $C_{7'}$-**H**), 6.95 (t, *J* = 8.0 Hz 1H, $C_{6'}$-**H**), 7.00 (d, *J* = 8.0 Hz, 1H, $C_{5'}$-**H**). ^{13}CNMR (100 MHz, $CDCl_3$) δ (ppm): 19.36 (2C, C_2-**CH_3**and C_6-**CH_3**), 34.62 (1C, **C_4**), 50.94 (2C, COO**CH_3**), 104.23 (2C, **C_3** and **C_5**), 107.14 (1C, **$C_{7'}$**), 112.78 (1C, **C**F_2), 123.21 (1C, **$C_{5'}$**), 124.20 (1C, **$C_{6'}$**), 132.48 (1C, **$C_{4'}$**), 143.34 (2C, ***C_2*** and **C_6**), 144.83 (1C, **$C_{3a'}$**), 148.99 (1C, **$C_{7a'}$**), 167.49 (2C, **C═O**).IR (KBr disc): $\tilde{\nu}$(cm^{-1}): 3316 (N—H Str), 2953 (aliphatic C—H Str), 1701 (C═O Str), 1646 (aliphatic C═C Str), 1491 (aromatic C═C), 1220 (aliphatic C—N Str), 774 (N—H Wag). EI-MS: *m/z* (% abundance): 380.85 (**M^+**, 3.08), 223.95 (**$M^+-C_7H_5F_2O_2$**,100.00). Elemental analysis (%) for $C_{18}H_{17}F_2NO_6$, calcd. (found):C 56.70 (56.43), H 4.49 (4.58), N 3.76 (3.61).

3.1.5. General Procedure for Preparation of DHP Derivatives (*9a,b*).

A mixture of acetoacetate esters **2c,d** (1.67 mmol), 2,3-(methylenedioxy)-benzaldehyde (0.250 g, 1.67 mmol) and alkyl 3-aminocrotonate (1.67 mmol) was dissolved in isopropanol (10 ml), and then heated under reflux for 6 h. The reaction mixture was quenched by the addition of dist. water (20 ml) and then cooled in an ice-bath. The precipitated solid was filtered and re-crystallized by methanol to afford products (**9a, b**).

*3-Tert-butyl 5-methyl 4-(2H-1,3-benzodioxol-4-yl)-2,6-dimethyl-1,4-dihydropyridine-3,5-dicarboxylate (**9a**).*

The general procedure mentioned above was applied using 2,3-(methylenedioxy)-benzaldehyde (0.250 g, 1.67 mmol), **2d** (0.264 g, 1.67 mmol) and methyl 3-aminocrotonate (0.192 g, 1.67 mmol) to afford 0.531 g, (82.3% yield) as pale-yellow crystals. R_f = 0.79 (chloroform: isopropanol(90:10)); mp 178–180 °C.^{1}H NMR (400 MHZ, $CDCl_3$) δ (ppm): 2.26 (s, 9H, C (**CH_3**)$_3$), 3.59 (s, 9H, C_2-**CH_3** , C_6-**CH_3** and O**CH_3**), 4.85 (s, 1H, **C_4**-H), 5.57 (s, 1H, NH), 5.81 (s, 2H, O**CH_2**O), 6.59 (d, *J* = 7.9 Hz, 1H, $C_{6'}$-**H**), 6.65 (t, *J* = 7.9 Hz, 1H, $C_{6'}$-**H**), 6.77 (d, *J* = 7.9 Hz, 1H, $C_{5'}$-**H**). ^{13}CNMR (100 MHz, $CDCl_3$) δ (ppm): 19.61 (2C, C_2-**CH_3** and C_6-**CH_3**), 28.35 (3C, C (**CH_3**)$_3$), 39.04 (1C, **C_4**), 51.00 (1C, O**CH_3**) , 88.78 (1C, **C**(CH_3)$_3$)100.65 (1C, O**CH_2**O), 104.08 (2C, **C_3** and **C_5**), 107.75 (1C, **$C_{7'}$**), 121.49 (1C, **$C_{5'}$**), 122.34 (1C, **$C_{6'}$**), 129.71 (1C, **$C_{4'}$**),143.93 (2C, ***C_2*** and **C_6**), 145.81 (1C, **$C_{3a'}$**), 147.31 (1C, **$C_{7a'}$**), 168.03 (2C, **2C = O**). IR (KBr disc): $\tilde{\nu}$(cm^{-1}): 3346 (N—H Str), 2980 (aliphatic C—H Str), 1698 (C═O Str), 1610 (aliphatic C═C Str), 1492 (aromatic C═C), 1242 (aliphatic C—N Str), 749 (N—H Wag). EI-MS: *m/z* (% abundance): 386.90 (**M^+**, 0.39), 223.90 (**$C_{11}H_{13}NO_4^+$**, 100). Elemental analysis (%) for $C_{21}H_{25}NO_6$, calcd. (found): C 65.10 (65.00), H 6.50 (6.35), N 3.62 (3.95).

3-Ethyl 5-isopropyl4-(2H-1,3-benzodioxol-4-yl)-2,6-dimethyl-1,4-

*dihydropyridine-3,5-dicarboxylate (**9b**).*

The general procedure mentioned above was applied using 2,3-(methylenedioxy)-benzaldehyde (0.250 g, 1.67 mmol), **2c** (0.241 g, 1.67 mmol) and ethyl 3-aminocrotonate (0.215 g, 1.67 mmol) to give 0.459 g, (69.99% yield) as pale-yellow crystals. $R_f = 0.74$ (chloroform: isopropanol(90:10)); mp 186–188 °C.^{1}HNMR (400 MHZ, $CDCl_3$) δ (ppm): 1.17 (d, $J = 6.3$ Hz, 6H, CH(**CH_3**)$_2$), 1.28 (t, $J = 7.4$ Hz, 3H, CH_2**CH_3**), 2.34 (s, 6H, C_2-**CH_3** and C_6-**CH_3**), 4.13 (q, $J = 7.1$ Hz ,2H, **CH_2**CH_3), 4.82 (s, 1H, C_4-**H**), 4.89–5.06 (m, $J = 6.5$ Hz, 1H, **CH**$(CH_3)_2$), 5.62 (s, 1H, NH) , 5.90 (s, 2H, O**CH_2**O), 6.63 (d, $J = 7.9$ Hz, 1H, $C_{6'}$-**H**), 6.67 (t, $J = 7.9$ Hz, 1H, $C_{6'}$-**H**), 6.80 (d, $J = 7.9$ Hz, 1H, $C_{5'}$-**H**).^{13}CNMR (100 MHZ, $CDCl_3$) δ (ppm): 14.29 (C, CH_2**CH_3**), 19.57 (2C, C_2-**CH_3**and C_6-**CH_3**), 22.13 (2C, CH(**CH_3**)$_2$), 39.43 (1C, **C_4**), 59.71 (1C, **CH_2**CH_3), 67.00 (1C, **CH**$(CH_3)_2$), 107.46 (1C, **$C_{7'}$**), 121.82 (1C, **$C_{5'}$**), 122.72 (1C, **$C_{6'}$**), 129.88 (1C, **$C_{4'}$**),143.20 (2C, ***C_2*** and **C_6**), 145.64 (1C, aromatic **$C_{3a'}$**), 147.14 (1C, **$C_{7a'}$**), 167.14 (2C, 2**C = O**). IR (KBr disc): $\tilde{\nu}$(cm^{-1}): 3331 (N—H Str), 2987 (aliphatic C—H Str), 1689 (C=O Str), 1649 (aliphatic C=C Str), 1500 (aromatic), 1219 (aliphatic C—N Str), 749 (N—H Wag). EI-MS: *m/z* (% abundance): 386.90 (**M$^+$**,10.82), 343.85 (**M$^+$−C_3H_7**, 17.51), 315.85 (**M$^+$−C_5H_{12}**, 20.34), 265.95 (**M$^+$−$C_7H_5O_2$**, 60.71), 195.90 (**M$^+$−$C_{12}H_{17}O_2$**, 100). Elemental analysis (%) for $C_{21}H_{25}NO_6$, calcd. (found): C 65.10 (64.80), H 6.50 (6.37), N 3.62 (3.42).

3.1.6. General Procedure for Preparation of DHP Derivatives (11a-c).

A mixture of acetoacetate esters **2a-c** (2.58 mmol), Fluorene-2-carboxaldehyde (0.250 g, 1.29 mmol) and ammonium acetate (0.162 g, 2.10 mmol) was dissolved in isopropanol (10 ml), and then heated under reflux for 6 h. The reaction mixture was quenched by the addition of dist. water (20 ml) and then cooled in an ice-bath. The precipitated solid was filtered and re-crystallized by methanol to afford products (**11a-c**).

*3,5-Dimethyl 4-(9H-fluoren-2-yl)-2,6-dimethyl-1,4-dihydropyridine-3,5-dicarboxylate (**11a**).*

Yield (0.479 g, 95.4%) as pale-yellow crystals. $R_f = 0.92$ (chloroform: isopropanol(90:10)); mp 242–244 °C.^{1}HNMR (400 MHz, $CDCl_3$) δ (ppm): 2.39 (s, 6H, C_2-**CH_3**and C_6-**CH_3**), 3.69 (s, 6H, COO**CH_3**), 3.85 (s, 2H, **CH_2**), 5.13 (s, 1H, C_4-**H**), 5.87 (s, 1H, NH) , 7.28 (dd, 1H, $J = 7.8$, 1.7 Hz, Fluorene C_4-**H**), 7.35 (t, 2H, $J = 7.9$ Hz, Fluorene C_6-**H** and C_7-**H**), 7.47 (s, 1H, Fluorene C_1-**H**), 7.52 (d, $J = 7.5$ Hz ,1H, Fluorene C_3-**H**), 7.65 (dd, 1H, $J = 7.8$, 1.7 Hz, Fluorene C_5-**H**), 7.74 (d, $J = 7.5$ Hz, 1H, Fluorene C_8-**H**). ^{13}CNMR (100 MHz, $CDCl_3$) δ (ppm): 19.65 (2C, C_2-**CH_3** and C_6-**CH_3**), 36.87(1C, **CH_2**), 39.50 (1C, **C_4**), 51.03 (2C, COO**CH_3**), 104.06 (2C, **C_3** and **C_5**), 119.37 (1C, Fluorene-**C_4**), 119.61 (1C, Fluorene-**C_6**), 124.32 (1C, Fluorene-**C_1**), 124.89 (1C, Fluorene-**C_8**), 126.31 (1C, Fluorene-**C_7**), 126.43 (1C, Fluorene-**C_3**), 126.59 (1C, Fluorene-**C_5**), 139.99 (1C, Fluorene-***C_2***) ,141.79 (1C, Fluorene-**C_{4b}**), 143.24 (1C, Fluorene-**C_{9a}**), 143.36 (1C, Fluorene-**C_{8a}**), 144.15 (1C, Fluorene-**C_{4a}**), 146.42 (2C, ***C_2*** and **C_6**), 168.16 (2C, 2**C = O**). IR (KBr disc):$\tilde{\nu}$ (cm^{-1}): 3349 (N—H Str), 2950 (aliphatic C—H Str), 1698 (C=O Str), 1651 (aliphatic C=C Str), 1487 (aromatic C=C), 1221 (aliphatic C—N Str), 738 (N—H Wag). EI-MS: *m/z* (% abundance): 388.90 (**M$^+$**, 4.79), 223.95 (**M$^+$−$C_{13}H_9$**,100.00). Elemental analysis (%) for $C_{24}H_{23}NO_4$, calcd. (found): C 74.02 (74.22), H 5.59(5.86), N 3.60 (3.82).

*3,5-Diethyl 4-(9H-fluoren-2-yl)-2,6-dimethyl-1,4-dihydropyridine-3,5-dicarboxylate (**11b**).*

Yield (0.465 g, 86.4%) as pale-yellow crystals. $R_f = 0.93$ (chloroform: isopropanol(90:10)); mp 249–251 °C.^{1}HNMR (400 MHz, $CDCl_3$) δ (ppm): 1.25 (t, $J = 7.1$ Hz, 6H, 2 of CH_2**CH_3**), 2.38 (s, 6H, C_2-**CH_3**and C_6-**CH_3**),3.85 (s, 2H, **CH_2**), 4.10 (m, $J = 7.1$ Hz ,4H, 2 of **CH_2**CH_3), 5.09 (s, 1H, C_4-**H**), 5.81 (s, 1H, **NH**) , 7.29 (dd, 1H, $J = 7.8$, 1.7 Hz, Fluorene C_4-**H**), 7.35 (t, 2H, $J = 7.9$ Hz, Fluorene C_6-**H** and C_7-**H**), 7.47 (s, 1H, Fluorene C_1-**H**), 7.53 (d, $J = 7.5$ Hz ,1H, Fluorene C_3-**H**), 7.66 (dd, 1H, $J = 7.8$, 1.7 Hz, Fluorene C_5-**H**), 7.74 (d, $J = 7.5$ Hz, 1H, Fluorene C_8-**H**). ^{13}CNMR (100 MHz, $CDCl_3$) δ (ppm): 14.29 (2C,CH_2**CH_3**), 19.63 (2C, C_2-**CH_3**and C_6-**CH_3**), 36.90(1C,**CH_2**),39.88 (1C, **C_4**), 59.74 (2C, **CH_2**CH_3), 104.33 (2C, **C_3** and **C_5**), 119.17 (1C, Fluorene-**C_4**), 119.57 (1C, Fluorene-**C_6**), 124.75 (1C, Fluorene-**C_1**), 124.88 (1C, Fluorene-**C_8**), 126.14 (1C, Fluorene-**C_7**), 126.57 (1C, Fluorene-**C_3**), 126.82 (1C, Fluorene-**C_5**), 139.80 (1C, Fluorene-***C_2***) ,141.87 (1C, Fluorene-**C_{4b}**), 142.94 (1C, Fluorene-**C_{9a}**), 143.35 (1C, Fluorene-**C_{8a}**), 143.76 (1C, Fluorene-**C_{4a}**), 146.82 (2C, ***C_2*** and **C_6**), 167.73 (2C, 2**C = O**). IR (KBr disc)$\tilde{\nu}$ (cm^{-1}): 3331 (N—H Str), 2947 (aliphatic C—H Str), 1658 (C=O Str), 1602 (aliphatic C=C Str), 1453 (aromatic), 1221 (aliphatic C—N Str), 735 (N—H Wag). EI-MS: *m/z* (% abundance): 417.25 (**M$^+$**, 9.69), 252.20 (**M$^+$−$C_{13}H_9$**,100.00). Elemental analysis (%) for $C_{26}H_{27}NO_4$, calcd. (found): C 74.80 (75.04), H 6.52(6.22), N 3.35 (2.98).

*3,5-Diisopropyl 4-(9H-fluoren-2-yl)-2,6-dimethyl-1,4-dihydropyridine −3,5-dicarboxylate (**11c**)*

Yield (0.508 g, 88.2%) as pale-yellow crystals. $R_f = 0.95$ (chloroform: isopropanol (90:10)); mp 244–247 °C. ^{1}HNMR (400 MHz, $CDCl_3$) δ (ppm): 1.12 (d, $J = 6.2$ Hz, 6H, CH(**CH_3**)$_2$), 1.19 (d, $J = 6.2$ Hz, 6H, CH (**CH_3**)$_2$), 2.35 (s, 6H, C_2-**CH_3** and C_6-**CH_3**), 3.85 (s, 2H, **CH_2**), 4.09 (s, 1H, C_4-**H**), 5.19 (m, $J = 6.5$ Hz ,2H, 2 of **CH**$(CH_3)_2$), 5.89 (s, 1H, NH), 7.30 (dd, 1H, $J = 7.8$, 1.7 Hz, Fluorene C_4-**H**), 7.39 (t, 2H, $J = 7.9$ Hz, Fluorene C_6-**H** and C_7-**H**), 7.49 (s, 1H, Fluorene C_1-**H**), 7.55 (d, $J = 7.5$ Hz ,1H, Fluorene C_3-**H**), 7.66 (dd, 1H, $J = 7.8$, 1.7 Hz, Fluorene C_5-**H**),7.71 (d, $J = 7.5$ Hz, 1H, Fluorene C_8-**H**). ^{13}C NMR ($CDCl_3$) δ(ppm): 19.34 (2C, C_2-**CH_3**and C_6-**CH_3**), 21.67 (2C, CH(**CH_3**)$_2$), 22.02 (2C, CH(**CH_3**)$_2$), 36.78(1C,**CH_2**), 39.34 (1C, **C_4**), 67.36 (2C, 2 of **CH**$(CH_3)_2$), 104.67 (2C, **C_3** and **C_5**), 119.11 (1C, Fluorene-**C_4**), 119.52 (1C, Fluorene-**C_6**), 124.66 (1C, Fluorene-**C_1**), 124.81 (1C, Fluorene-**C_8**), 126.13 (1C, Fluorene-**C_7**), 126.54 (1C, Fluorene-**C_3**), 126.80 (1C, Fluorene-**C_5**), 139.80 (1C, Fluorene-***C_2***) ,141.85 (1C, Fluorene-**C_{4b}**), 142.91 (1C, Fluorene-**C_{9a}**), 143.33 (1C, Fluorene-**C_{8a}**), 143.72 (1C, Fluorene-**C_{4a}**), 146.81 (2C, ***C_2*** and **C_6**), 167.74 (2C, 2**C = O**). IR (KBr disc): $\tilde{\nu}$(cm^{-1}): 3331 (N—H Str), 2947 (aliphatic C—H Str), 1658 (C=O Str), 1602 (aliphatic C=C Str), 1453 (aromatic), 1221 (aliphatic C—N Str), 735 (N—H Wag). EI-MS: *m/z* (% abundance): 444.85 (**M$^+$**, 8.65), 279.95 (**M$^+$−$C_{13}H_9$**, 100.00). Elemental analysis (%) for $C_{28}H_{31}NO_4$,calcd. (found): C 75.48 (75.29), H 7.01(7.30), N 3.14 (3.42).

3.1.7. General Procedure for Preparation of DHP Derivatives (13a-c)

A mixture of acetoacetate esters **2a-c** (3.04 mmol), 1,4-Benzodioxan-6-carboxaldehyde (0.250 g, 1.52 mmol) and ammonium acetate (0.162 g, 2.10 mmol) was dissolved in isopropanol (10 ml), and then heated under reflux for 6 h. The reaction mixture was quenched by the addition of dist. water (20 ml) and then cooled in an ice-bath. The precipitated solid was filtered and re-crystallized by methanol to afford products (**13a-c**).

*3,5-Dimethyl 4-(2,3-dihydro-1,4-benzodioxin-6-yl)-2,6-dimethyl-1,4-dihydropyridine-3,5-dicarboxylate (**13a**)*

Yield (0.531 g, 90.1%) as pale-yellow crystals. $R_f = 0.69$ (chloroform: isopropanol (90:10)); mp 214–216 °C. ^{1}HNMR (400 MHZ, $CDCl_3$) δ (ppm): 2.35 (s, 6H, C_2-**CH_3**and C_6-**CH_3**), 3.69 (s, 6H, COO**CH_3**), 4.23 (s, 4H, –C**H_2**C**H_2**-), 4.93 (s, 1H, C_4-**H**), 5.64 (s, 1H, NH), 6.71–6.73 (m, 1H, $C_{5'}$-**H**), 6.76–6.79 (m, 2H, $C_{7'}$-**H** and $C_{8'}$-**H**). ^{13}CNMR (100 MHz, $CDCl_3$) δ (ppm): 19.61 (2C, C_2-**CH_3**and C_6-**CH_3**), 38.47 (1C, **C_4**), 51.00 (2C, COO**CH_3**), 64.29(1C, **C**H_2O), 64.37(1C, O**C**H_2), 103.99 (2C, **C_3** and **C_5**), 116.23 (1C, **$C_{5'}$**), 116.60 (1C, **$C_{8'}$**), 120.69 (1C, **$C_{7'}$**), 140.99 (1C, **$C_{6'}$**), 141.97 (1C, **$C_{4a'}$**), 143.01 (1C, aromatic **$C_{8a'}$**), 143.97 (2C, ***C_2*** and **C_6**), 168.02 (2C,2**C = O**). IR (KBr disc): $\tilde{\nu}$ (cm^{-1}): 3339 (N—H Str), 2951 (aliphatic C—H Str), 1696 (C=O Str), 1649 (aliphatic C=C Str), 1495 (aromatic), 1223 (aliphatic C—N Str), 750 (N—H Wag). EI-MS: *m/z* (% abundance): 358.90 (**M$^+$**, 6.68), 223.95 (**M$^+$−$C_8H_7O_2$**,100.00). Elemental analysis (%) for $C_{19}H_{21}NO_6$, calcd. (found):C 63.50 (63.29), H 5.89 (5.81), N 3.90 (3.91).

*3,5-Diethyl4-(2,3-dihydro-1,4-benzodioxin-6-yl)-2,6-dimethyl-1,4-dihydropyridine-3,5-dicarboxylate (**13b**).*

Yield (0.509 g, 86.4%) as pale-yellow crystals. $R_f = 0.67$ (chloroform: isopropanol(90:10)); mp 195–197 °C. ^{1}HNMR (400 MHz, $CDCl_3$) δ (ppm): 1.26 (t, $J = 7.2$ Hz, 6H, 2 of CH_2**CH_3**), 2.34 (s, 6H, C_2-**CH_3**and C_6-**CH_3**), 4.11–4.21 (m, 4H, 2 of C**H_2**CH_3), 4.23(s, 4H, –C**H_2**C**H_2**-), 4.92 (s,

1H, C_4-**H**), 5.63 (s, 1H, NH), 6.67–6.74 (m, 1H, $C_{5'}$-**H**), 6.76–6.83 (m, 2H, $C_{7'}$-**H** and $C_{8'}$-**H**). ^{13}C NMR ($CDCl_3$) δ (ppm): 14.29 (2C, CH_2**CH_3**), 19.59 (2C, C_2-**CH_3**and C_6-**CH_3**), 38.81(1C, **C_4**), 59.71 (2C, **CH_2**CH_3), 64.31(1C, **CH_2**O), 64.36(1C, O**CH_2**), 104.25 (2C, **C_3** and **C_5**), 116.32 (1C, **$C_{5'}$**), 116.57 (1C, **$C_{8'}$**), 121.10 (1C, **$C_{7'}$**), 141.37 (1C, **$C_{6'}$**), 141.88 (1C, **$C_{4a'}$**), 142.94 (1C, **$C_{8a'}$**), 143.61 (2C, **C_2** and **C_6**), 167.64 (2C, 2**C** = **O**). IR (KBr disc): $\tilde{\nu}$ (cm^{-1}): 3324 (N—H Str), 2984 (aliphatic C—H Str), 1691 (C═O Str), 1649 (aliphatic C═C Str), 1498 (aromatic C═C), 1216 (aliphatic C—N Str), 748 (N—H Wag). EI-MS: *m/z* (% abundance): 368.90 (**M^+**, 9.98), 251.90 (**$M^+-C_8H_7O_2$**,100.00). Elemental analysis (%) for $C_{21}H_{25}NO_6$, calcd. (found):C 65.10 (65.41), H 6.50 (6.60), N 3.62 (3.88).

*3,5-Diisopropyl 4-(2,3-dihydro-1,4-benzodioxin-6-yl)-2,6-dimethyl-1,4-dihydropyridine-3,5-dicarboxylate (**13c**).*

Yield (0.520 g, 82.3%) as pale-yellow crystals. $R_f = 0.69$ (chloroform: isopropanol(90:10));mp 190–192 °C. ^{1}HNMR (400 MHz, $CDCl_3$) δ (ppm): 1.18 (d, $J = 6.2$ Hz, 6H, CH(**CH_3**)$_2$), 1.28 (d, $J = 6.2$ Hz, 6H, CH(**CH_3**)$_2$), 2.33 (s, 6H, C_2-**CH_3** and C_6-**CH_3**), 4.23 (s, 4H, –**CH_2CH_2**-), 4.89 (s, 1H, C_4-**H**), 4.94–5.06 (m, $J = 6.5$ Hz ,2H, 2 of **CH**(CH_3)$_2$), 5.54 (s, 1H, NH), 6.71 (d, $J = 8.2$ Hz, $C_{8'}$-**H**), 6.79 (d, $J = 8.0$ Hz, 1H, $C_{7'}$-**H**), 6.80 (s, 1H, $C_{5'}$-**H**). ^{13}C NMR ($CDCl_3$) δ (ppm): 19.60 (2C, C_2-**CH_3** and C_6-**CH_3**), 21.87 (2C, CH(**CH_3**)$_2$), 22.13 (2C, CH(**CH_3**)$_2$), 38.99 (1C, **C_4**), 64.35(1C, **CH_2**O), 66.93(1C, O**CH_2**), 104.60 (2C, **C_3** and **C_5**), 116.10 (1C, **$C_{5'}$**), 116.76 (1C, **$C_{8'}$**), 121.36 (1C, **$C_{7'}$**), 141.52 (1C, aromatic **$C_{6'}$**), 141.79 (1C, **$C_{4a'}$**), 142.87 (1C, **$C_{8a'}$**), 143.20 (2C, **C_2**and **C_6**), 167.16 (2C, 2**C** = **O**). IR (KBr disc) $\tilde{\nu}$ (cm^{-1}): 3346 (N—H Str), 2980 (aliphatic C—H Str), 1691 (C═O Str), 1653 (aliphatic C═C Str), 1494 (aromatic C═C), 1213 (aliphatic C—N Str), 759 (N—H Wag). EI-MS: *m/z* (% abundance): 414.90 (**M^+**, 15.15), 279.95 (**$M^+-C_8H_7O_2$**,100), 237.90 (**$M^+-C_{11}H_{13}O_2$**, 43.93), 195.90 (**$M^+-C_{14}H_{19}O_2$**, 98.52). Elemental analysis (%) for $C_{23}H_{29}NO_6$, calcd. (found): C 66.49 (66.71), H 7.04 (7.28), N 3.37 (3.16).

Full descriptions of biological and CADD methods are provided in the Supporting Information.

4. Conclusion

1.4-DHPs with a lipophilic aldehydic core and smaller side chains, preferably the ethyl side chains, show a better anticancer profile than hydrophilic ones. Molecularly, DHPs anticipate simultaneously TOPI and RTKs (VEGFR-2, HER-2 and BTK). This leads to the accumulation of DNA cleavable complexes which can trigger the intrinsic apoptotic pathway by stimulating BAX/BAK and the following cascades ends with executioner caspases. On the other hand, blocking the intracellular tyrosine kinase domain of RTKs hinders the activation of the oncogenic pathways (PI3K, AKT, RAS and MAPK) which directly affect the tumorigenesis process.

Declaration of Competing Interest

The authors declare that they have no known competing financial interests or personal relationships that could have appeared to influence the work reported in this paper.

Acknowledgment

Yusuf A. Haggag (Faculty of Pharmacy-Tanta University) is acknowledged for the *in vivo* antitumor experimental work. Also, we thank Ahmed S. (Faculty of Pharmacy-Tanta University) and Shaimaa M. Aboukhatwa (Department of Medicinal Chemistry and Pharmacognosy, College of Pharmacy, University of Illinois, Chicago) for helping in the CADD work. Finally, we thank the referees for their insightful comments and suggestions.

Author Information

The manuscript was written through contributions of all authors. All authors have given approval to the final version of the manuscript.

Funding

This research did not receive any specific grant from funding agencies in the public, commercial or not-for-profit sectors.

Appendix A. Supplementary data

Supplementary data (Spectral data (^{1}H NMR, ^{13}C- NMR, IR and EI-MS) for each compound; Details of the preliminary SAR study of DHPs as anticancer agents; GI% of our candidates over 18 cancer and 9 human normal cell lines; spectrum table for DHPs as anticancer agents; GI_{50} of **11b** over 18 cancer and 9 normal cell lines with the SI; Cell cycle analysis and apoptosis percentages on A549 and MDA-MB-468 cell lines; In-silico Pharmacokinetics and Druglikeness Properties' Prediction; all 2D and 3D docking figures used in the manuscript; all experimental methods used in the biological evaluation and CADD. This material is available free of charge and can be found online at https://doi.org/10.1016/j.bioorg.2021.105054.

References

[1] J. Stocklöv, Arthur Rudolf, *Hantzsch imBriefwechselmit Wilhelm Ostwald*. ERS-Verlag (1998).
[2] A. Hantzsch, CondensationsprodukteausAldehydammoniak und ketonartigenVerbindungen, Berichte der deutschenchemischen Gesellschaft 14 (2) (1881) 1637–1638.
[3] D.M. Stout, A. Meyers, Recent advances in the chemistry of dihydropyridines, Chemical reviews 82 (2) (1982) 223–243.
[4] A.P. Phillips, Hantzsch's pyridine synthesis, Journal of the American Chemical Society 71 (12) (1949) 4003–4007.
[5] Grün, G.; Fleckenstein, A., Electromechanical uncoupling of vascular smooth muscle as the basic principle of coronary dilatation by 4-(2'-nitrophenyl-2, 6-dimethyl-1, 4-dihydropyridine-3, 5-dicarboxylic acid dimethyl ester (BAY a 1040, Nifedipine). 1. The significance of Ca++ ions for the bioelectrical and mechanical activity of smooth muscle. Arzneimittel-Forschung1972,22 (2), 334.
[6] P. Fatt, B. Katz, The electrical properties of crustacean muscle fibres, The Journal of Physiology 120 (1–2) (1953) 171–204.
[7] P. Fatt, B. Ginsborg, The ionic requirements for the production of action potentials in crustacean muscle fibres, The Journal of Physiology 142 (3) (1958) 516–543.
[8] B. Katz, R. Miledi, A study of synaptic transmission in the absence of nerve impulses, The Journal of Physiology 192 (2) (1967) 407–436.
[9] H. Reuter, The dependence of slow inward current in Purkinje fibres on the extracellular calcium-concentration, The Journal of Physiology 192 (2) (1967) 479–492.
[10] S. Hagiwara, S. Ozawa, O. Sand, Voltage clamp analysis of two inward current mechanisms in the egg cell membrane of a starfish, The Journal of General Physiology 65 (5) (1975) 617–644.
[11] Kohlhardt, M.; Bauer, B.; Krause, H.; Fleckenstein, A., Differentiation of the transmembrane Na and Ca channels in mammalian cardiac fibresby the use of specific inhibitors. PflügersArchiv1972,335 (4), 309-322.
[12] M. Kohlhardt, B. Bauer, H. Krause, A. Fleckenstein, New selective inhibitors of the transmembrane Ca conductivity in mammalian myocardial fibres. Studies with the voltage clamp technique, Experientia 28 (3) (1972) 288–289.
[13] Kohlhardt, M.; Fleckenstein, A., Inhibition of the slow inward current by nifedipine in mammalian ventricular myocardium. Naunyn-Schmiedeberg'sArchives of Pharmacology 1977,298 (3), 267-272.
[14] A. Fleckenstein, History of calcium antagonists, Circulation Research 52 (2 Pt 2) (1983) I3–16.
[15] S. Valente, P. Mellini, F. Spallotta, V. Carafa, A. Nebbioso, L. Polletta, I. Carnevale, S. Saladini, D. Trisciuoglio, C. Gabellini, 1, 4-Dihydropyridines active on the SIRT1/AMPK pathway ameliorate skin repair and mitochondrial function and exhibit inhibition of proliferation in cancer cells, Journal of Medicinal Chemistry 59 (4) (2016) 1471–1491.
[16] M.F. Mohamed, A.F. Darweesh, A.H. Elwahy, I.A. Abdelhamid, Synthesis, characterization and antitumor activity of novel tetrapodal 1, 4-dihydropyridines: p53 induction, cell cycle arrest and low damage effect on normal cells induced by genotoxic factor H 2 O 2, RSC Advances 6 (47) (2016) 40900–40910.
[17] M.F. Mohamed, N.S. Ibrahim, A.H. Elwahy, I.A. Abdelhamid, Molecular Studies on Novel Antitumor Bis 1, 4-Dihydropyridine Derivatives Against Lung Carcinoma and their Limited Side Effects on Normal Melanocytes, Anti-Cancer Agents in Medicinal Chemistry (Formerly Current Medicinal Chemistry-Anti-Cancer Agents) 18 (15) (2018) 2156–2168.

[18] G. Prasanthi, K. Prasad, K. Bharathi, Synthesis, anticonvulsant activity and molecular properties prediction of dialkyl 1-(di (ethoxycarbonyl) methyl)-2, 6-dimethyl-4-substituted-1, 4-dihydropyridine-3, 5-dicarboxylates, European Journal of Medicinal Chemistry 73 (2014) 97–104.

[19] G. Prasanthi, K. Prasad, K. Bharathi, Design, synthesis and evaluation of dialkyl 4-(benzo [d][1, 3] dioxol-6-yl)-1, 4-dihydro-2, 6-dimethyl-1-substituted pyridine-3, 5-dicarboxylates as potential anticonvulsants and their molecular properties prediction, European Journal of Medicinal Chemistry 66 (2013) 516–525.

[20] M.S. Saddala, R. Kandimalla, P.J. Adi, S.S. Bhashyam, U.R. Asupatri, Novel 1, 4-dihydropyridines for L-type calcium channel as antagonists for cadmium toxicity, Scientific Reports 7 (2017) 45211.

[21] E. Praveenkumar, N. Gurrapu, P.K. Kolluri, V. Yerragunta, B.R. Kunduru, N. Subhashini, Synthesis, anti-diabetic evaluation and molecular docking studies of 4-(1-aryl-1H-1, 2, 3-triazol-4-yl)-1, 4-dihydropyridine derivatives as novel 11-β hydroxysteroid dehydrogenase-1 (11β-HSD1) inhibitors, Bioorganic Chemistry 90 (2019), 103056.

[22] H. Yousuf, S. Shamim, K.M. Khan, S. Chigurupati, S. Hameed, M.N. Khan, M. Taha, M. Arfeen, Dihydropyridines as potential α-amylase and α-glucosidase inhibitors: synthesis, in vitro and in silico studies, Bioorganic Chemistry 96 (2020), 103581.

[23] H. Niaz, H. Kashtoh, J.A. Khan, A. Khan, M.T. Alam, K.M. Khan, S. Perveen, M. I. Choudhary, Synthesis of diethyl 4-substituted-2, 6-dimethyl-1, 4-dihydropyridine-3, 5-dicarboxylates as a new series of inhibitors against yeast α-glucosidase, European Journal of Medicinal Chemistry 95 (2015) 199–209.

[24] S. Ulloora, R. Shabaraya, R. Ranganathan, A.V. Adhikari, Synthesis, anticonvulsant and anti-inflammatory studies of new 1, 4-dihydropyridin-4-yl-phenoxyacetohydrazones, European Journal of Medicinal Chemistry 70 (2013) 341–349.

[25] A.A. Eissa, N.A. Farag, G.A. Soliman, Synthesis, biological evaluation and docking studies of novel benzopyranone congeners for their expected activity as anti-inflammatory, analgesic and antipyretic agents, Bioorganic & Medicinal Chemistry 17 (14) (2009) 5059–5070.

[26] R. Malek, R.L. Arribas, A. Palomino-Antolin, P. Totoson, C. Demougeot, T. Kobrlova, O. Soukup, I. Iriepa, I. Moraleda, D. Diez-Iriepa, New Dual Small Molecules for Alzheimer's Disease Therapy Combining Histamine H3 Receptor (H3R) Antagonism and Calcium Channels Blockade with Additional Cholinesterase Inhibition, Journal of Medicinal Chemistry 62 (24) (2019) 11416–11422.

[27] W. Report, WHO Cancer Report (2019).

[28] Organization, W. H., Cancer Country Profiles 2018; 2020. URL http://www. who. int/cancer/country-profiles/en/# E.

[29] P. Anaikutti, P. Makam, Dual active 1, 4-dihydropyridine derivatives: Design, green synthesis and in vitro anti-cancer and anti-oxidant studies, Bioorganic Chemistry 105 (2020), 104379.

[30] C. Coburger, J. Wollmann, M. Krug, C. Baumert, M. Seifert, J. Molnár, H. Lage, A. Hilgeroth, Novel structure–activity relationships and selectivity profiling of cage dimeric 1, 4-dihydropyridines as multidrug resistance (MDR) modulators, Bioorganic & Medicinal Chemistry 18 (14) (2010) 4983–4990.

[31] K. Sirisha, M.C. Shekhar, K. Umasankar, P. Mahendar, A. Sadanandam, G. Achaiah, V.M. Reddy, Molecular docking studies and in vitro screening of new dihydropyridine derivatives as human MRP1 inhibitors, Bioorganic & Medicinal Chemistry 19 (10) (2011) 3249–3254.

[32] V. Hulubei, S.B. Meikrantz, D.A. Quincy, T. Houle, J.I. McKenna, M.E. Rogers, S. Steiger, N. Natale, 4-Isoxazolyl-1, 4-dihydropyridines exhibit binding at the multidrug-resistance transporter, Bioorganic & Medicinal Chemistry 20 (22) (2012) 6613–6620.

[33] C. Baumert, M. Günthel, S. Krawczyk, M. Hemmer, T. Wersig, A. Langner, J. Molnár, H. Lage, A. Hilgeroth, Development of small-molecule P-gp inhibitors of the N-benzyl 1, 4-dihydropyridine type: Novel aspects in SAR and bioanalytical evaluation of multidrug resistance (MDR) reversal properties, Bioorganic & Medicinal Chemistry 21 (1) (2013) 166–177.

[34] A. Radadiya, V. Khedkar, A. Bavishi, H. Vala, S. Thakrar, D. Bhavsar, A. Shah, E. Coutinho, Synthesis and 3D-QSAR study of 1, 4-dihydropyridine derivatives as MDR cancer reverters, European Journal of Medicinal Chemistry 74 (2014) 375–387.

[35] F. Shekari, H. Sadeghpour, K. Javidnia, L. Saso, F. Nazari, O. Firuzi, R. Miri, Cytotoxic and multidrug resistance reversal activities of novel 1, 4-dihydropyridines against human cancer cells, European Journal of Pharmacology 746 (2015) 233–244.

[36] O. Shahraki, F. Zargari, N. Edraki, M. Khoshneviszadeh, O. Firuzi, R. Miri, Molecular dynamics simulation and molecular docking studies of 1, 4-Dihydropyridines as P-glycoprotein's allosteric inhibitors, Journal of Biomolecular Structure and Dynamics 36 (1) (2018) 112–125.

[37] G.R. Monteith, D. McAndrew, H.M. Faddy, S.J. Roberts-Thomson, Calcium and cancer: targeting Ca^{2+} transport, Nature Reviews Cancer 7 (7) (2007) 519–530.

[38] H.L. Roderick, S.J. Cook, Ca 2+ signalling checkpoints in cancer: remodelling Ca 2+ for cancer cell proliferation and survival, Nature Reviews Cancer 8 (5) (2008) 361–375.

[39] G.R. Monteith, N. Prevarskaya, S.J. Roberts-Thomson, The calcium–cancer signalling nexus, Nature Reviews Cancer 17 (6) (2017) 367.

[40] Meyer, V. H., Syntheseund vergleichendepharmakologischeuntersuchungen von 1, 4-dihydro-2, 6-dimethyl-4-(3 nitrophenyl) pyridin-3, 5-dicarbonsaeureestern mitnicht-identischenesterfunktionen. 1981.

[41] N.M. Evdokimov, I.V. Magedov, A.S. Kireev, A. Kornienko, One-step, three-component synthesis of pyridines and 1, 4-dihydropyridines with manifold medicinal utility, Organic Letters 8 (5) (2006) 899–902.

[42] Hyatt, J. A.; Feldman, P. L.; Clemens, R. J., Ketenes. 20. Thermal decomposition of 2, 2, 6-trimethyl-4H-1, 3-dioxin-4-one and 1-ethoxybutyn-3-one. Acetylketene. The Journal of Organic Chemistry 1984,49 (26), 5105-5108.

[43] M. Khoshneviszadeh, N. Edraki, K. Javidnia, A. Alborzi, B. Pourabbas, J. Mardaneh, R. Miri, Synthesis and biological evaluation of some new 1, 4-dihydropyridines containing different ester substitute and diethyl carbamoyl group as anti-tubercular agents, Bioorganic & Medicinal Chemistry 17 (4) (2009) 1579–1586.

[44] S. Parasuraman, Toxicological screening, Journal of Pharmacology & Pharmacotherapeutics 2 (2) (2011) 74.

[45] H.O. Tawfik, M.H. El-Hamamsy, N.A. Sharafeldin, T.F. El-Moselhy, Design, synthesis, and bioactivity of dihydropyrimidine derivatives as kinesin spindle protein inhibitors, Bioorganic & Medicinal Chemistry 27 (23) (2019), 115126.

[46] R.B. Badisa, S.F. Darling-Reed, P. Joseph, J.S. Cooperwood, L.M. Latinwo, C. B. Goodman, Selective cytotoxic activities of two novel synthetic drugs on human breast carcinoma MCF-7 cells, Anticancer Research 29 (8) (2009) 2993–2996.

[47] Z. Ullah, C.Y. Lee, M.L. DePamphilis, Cip/Kip cyclin-dependent protein kinase inhibitors and the road to polyploidy, Cell Division 4 (1) (2009) 10.

[48] B.G. Katzung, A.J. Trevor, Basic & clinical pharmacology, McGraw-Hill Education New York:, 2015.

[49] U. Eisner, J. Kuthan, Chemistry of dihydropyridines, Chemical Reviews 72 (1) (1972) 1–42.

[50] Andersen, M. H.; Becker, J. C.; thorStraten, P., Regulators of apoptosis: suitable targets for immune therapy of cancer. Nature Reviews Drug Discovery 2005,4 (5), 399-409.

[51] D.W. Meek, Tumour suppression by p53: a role for the DNA damage response? Nature Reviews Cancer 9 (10) (2009) 714–723.

[52] Y.A. Haggag, K.B. Matchett, R.A. Falconer, M. Isreb, J. Jones, A. Faheem, P. McCarron, M. El-Tanani, Novel ran-RCC1 inhibitory peptide-loaded nanoparticles have anti-cancer efficacy in vitro and in vivo, Cancers 11 (2) (2019) 222.

[53] A.B. Ibrahim, H.F. Zaki, W. Wadie, M.M. Omran, S.A. Shouman, Simvastatin Evokes An Unpredicted Antagonism For Tamoxifen In MCF-7 Breast Cancer Cells, Cancer Management and Research 11 (2019) 10011.

[54] A. Daina, O. Michielin, V. Zoete, SwissADME: a free web tool to evaluate pharmacokinetics, drug-likeness and medicinal chemistry friendliness of small molecules, Scientific Reports 7 (2017) 42717.

[55] C.A. Lipinski, F. Lombardo, B.W. Dominy, P.J. Feeney, Experimental and computational approaches to estimate solubility and permeability in drug discovery and development settings, Advanced Drug Delivery Reviews 23 (1–3) (1997) 3–25.

[56] W.J. Egan, K.M. Merz, J.J. Baldwin, Prediction of drug absorption using multivariate statistics, Journal of Medicinal Chemistry 43 (21) (2000) 3867–3877.

[57] I. Muegge, S.L. Heald, D. Brittelli, Simple selection criteria for drug-like chemical matter, Journal of Medicinal Chemistry 44 (12) (2001) 1841–1846.

[58] D.F. Veber, S.R. Johnson, H.-Y. Cheng, B.R. Smith, K.W. Ward, K.D. Kopple, Molecular properties that influence the oral bioavailability of drug candidates, Journal of medicinal chemistry 45 (12) (2002) 2615–2623.

[59] J. March, Advanced organic chemistry: reactions, mechanisms, and structure, John Wiley & Sons, 1992.

[60] M. McGann, FRED pose prediction and virtual screening accuracy, Journal of Chemical Information and Modeling 51 (3) (2011) 578–596.

[61] P.C. Hawkins, A.G. Skillman, G.L. Warren, B.A. Ellingson, M.T. Stahl, Conformer generation with OMEGA: algorithm and validation using high quality structures from the Protein Databank and Cambridge Structural Database, Journal of Chemical Information and Modeling 50 (4) (2010) 572–584.

[62] Soren, B. C.; Dasari, J. B.; Ottaviani, A.; Iacovelli, F.; Fiorani, P., Topoisomerase IB: a relaxing enzyme for stressed DNA.

[63] N.R. Brown, S. Korolchuk, M.P. Martin, W.A. Stanley, R. Moukhametzianov, M. E. Noble, J.A. Endicott, CDK1 structures reveal conserved and unique features of the essential cell cycle CDK, Nature Communications 6 (1) (2015) 1–12.

[64] C. Mao, M. Zhou, F.M. Uckun, Crystal structure of Bruton's tyrosine kinase domain suggests a novel pathway for activation and provides insights into the molecular basis of X-linked agammaglobulinemia, Journal of Biological Chemistry 276 (44) (2001) 41435–41443.

[65] M.M. Sultan, R.A. Denny, R. Unwalla, F. Lovering, V.S. Pande, Millisecond dynamics of BTK reveal kinome-wide conformational plasticity within the apo kinase domain, Scientific Reports 7 (1) (2017) 1–11.

[66] T. Ishikawa, M. Seto, H. Banno, Y. Kawakita, M. Oorui, T. Taniguchi, Y. Ohta, T. Tamura, A. Nakayama, H. Miki, Design and synthesis of novel human epidermal growth factor receptor 2 (HER2)/epidermal growth factor receptor (EGFR) dual inhibitors bearing a pyrrolo [3, 2-d] pyrimidine scaffold, Journal of Medicinal Chemistry 54 (23) (2011) 8030–8050.

[67] K. Aertgeerts, R. Skene, J. Yano, B.-C. Sang, H. Zou, G. Snell, A. Jennings, K. Iwamoto, N. Habuka, A. Hirokawa, Structural analysis of the mechanism of inhibition and allosteric activation of the kinase domain of HER2 protein, Journal of Biological Chemistry 286 (21) (2011) 18756–18765.

[68] K. Okamoto, M. Ikemori-Kawada, A. Jestel, K. von König, Y. Funahashi, T. Matsushima, A. Tsuruoka, A. Inoue, J. Matsui, Distinct binding mode of multikinase inhibitor lenvatinib revealed by biochemical characterization, ACS Medicinal Chemistry letters 6 (1) (2015) 89–94.